Muñoz, G., Mateus, A., Pous, J., Heise, W., Santos, F. M., Almeida, E. (2008): Unraveling middle-crust conductive layers in Paleozoic Orogens through 3D modeling of magnetotelluric data: The Ossa-Morena Zone case study (SW Iberian Variscides). - Journal of Geophysical Research, 113, B06106, 1-23

DOI: 10.1029/2007JB004987.

Unraveling middle-crust conductive layers in Paleozoic Orogens through 3D modeling of magnetotelluric data; the Ossa-Morena Zone case study (SW Iberian Variscides)

Gerard Muñoz [(1,+], Antonio Mateus[(2], Jaume Pous[(1], Wiebke Heise[(1,*], Fernando Monteiro Santos[(3], Eugenio Almeida[(4

[(1] Departament de Geodinàmica i Geofísica. Universitat de Barcelona. Martí Franquès s/n, 08028 Barcelona, Spain
[(2] Departamento de Geologia and CEGUL, Faculdade de Ciências da Universidade de Lisboa, C6, Piso 4, Campo Grande, 1749-016 Lisbon, Portugal
[(3] Faculdade de Ciências da Universidade de Lisboa, CGUL-IDL, C8, Piso 6, Campo Grande, 1749-016 Lisbon, Portugal
[(4] Instituto Politécnico de Tomar, Escola Superior de Tecnología de Tomar, 2300 Tomar, Portugal

+) Now at: GeoForschungsZentrum Potsdam. Telegrafenberg, 14473 Potsdam, Germany
*) Now at: GNS Science. PO Box 30368, Lower Hutt, New Zealand.

Abstract

In recent years a number of magnetotelluric (MT) surveys have been carried out in the southern branch of the Iberian Variscan Massif, namely in the Ossa Morena Zone (OMZ) and its neighboring areas, the South Portuguese Zone (SPZ) and the Central Iberian Zone (CIZ), in order to determine the geoelectrical structure of this transpressive orogen and gain insight into its internal architecture. New MT data collected across the OMZ complete a dense database that covers the whole belt and its boundaries. This paper presents an integrative three-dimensional model of the available MT data from the apparent resistivities (four components), impedance phases and geomagnetic transfer functions from 61 stations. Given the location of the study area, near the Atlantic Ocean, coast effect on the data was analyzed as well as the stability of the mesh due to the strong resistivity contrasts. A mesh of 80 x 77 x 76 cells was finally used, with an average cell size of 4 x 4 km in the horizontal direction, and increasing thickness in the vertical direction from 25 m in the shallower layers to 5 km in the deepest ones. The most striking feature is, in addition to the conductive anomalies associated with the sutures between the SPZ-OMZ and the OMZ-CIZ, a conductive layer which spans the whole Ossa Morena mid- to lower crust. The top of this conductive layer is interpreted as a major *décollement* between the granulitic basement and the overlying meta-sedimentary pile.

Keywords: Magnetotellurics, three-dimensional modeling, transpressive orogen, SW Iberia crustal structure

1. Introduction

The presence of mid-crustal conductive layers is known in many different geological settings. Regardless of the actual conductivity distribution, the available data show that a general conductivity pattern with depth is apparent: moderately to highly conductive shallow levels above highly resistive intermediate crustal layers beneath which conductivity increases again. (e.g., Egbert and Booker, 1992; Jones 1998, Eisel and Haak, 1999; Wannamaker, 2000). On the other hand, discontinuous conductive layers are frequently found within many middle crust resistive zones (e.g., Wannamaker et al., 2002; Tauber et al., 2003). In this context, the limited amount of interstitial aqueous fluids and the physical properties of minerals stable at intermediate continental crust levels can account for the conductive behavior. The conductive layers are therefore interpreted as related to important structural features (such as regional detachments) and/or particular rock compositions, probably enriched in fluid-deposited graphite and in solid carbon interconnected particles, either amorphous or as graphite (Monteiro Santos et al., 2002), or even in interconnected sulphides (Jones et al., 1997; Evans et al., 2005). The combination of these factors can therefore contribute to develop the particular conductivity distribution, and understanding the role played by each component is crucial for the interpretation of the conductivity models obtained.

In SW Iberia, an important segment of the Variscan fold-thrust belt can be characterized in detail, comprising three main geotectonic units: the Ossa Morena Zone (OMZ), the Central Iberian Zone (CIZ) and the South Portuguese Zone (SPZ). The OMZ corresponds to the internal continental segment of SW Iberian Variscides, and a number of MT surveys have been carried out in the last decade (Monteiro Santos el al., 1999; Almeida et al., 2001, 2005; Pous et al., 2004; Muñoz et al., 2005) to obtain data on: (1) the characterization of the electrical conductivity distribution of the whole crust in this transpressive orogen; (2) the detection of the tectonic structures responsible for the OMZ architecture, namely the main fault zones and *décollements*; and (3) the depiction of the north and south boundaries of the OMZ in depth. In the present work, new data complete a dense MT database in the SW Iberian Peninsula that was interpreted by three-dimensional (3D) forward modeling. The 3D model allows us to obtain an overall view of the conductivity distribution for the whole OMZ and its complex borders. Additionally, by considering together the geological and geophysical features, the role played by *décollement* tectonics in strain partitioning within the lithosphere during the SW Iberian Variscides development will be discussed.

Traditionally, many MT data sets have been interpreted with one-dimensional (1D) or two-dimensional (2D) techniques due to the heavy computational requirements of a 3D analysis. However, in recent years the 3D interpretation of MT data is becoming more common. Three-dimensional forward modeling is routinely used in diverse geological settings (e.g. Simpson 2000; Hoffmann Rothe et al., 2001; Varentsov et al., 2002) and although different 3D inversion algorithms have been published (e.g. Mackie and Madden, 1993; Sasaki, 2004; Avdeev, 2005; Siripunvaraporn et al., 2005) these are applied only in simple resistivity structures and are not yet in universal use. The present paper presents an unusually large and complex three-dimensional model, both in terms of area covered and complexity of the modeled structures.

2. The Ossa Morena Zone case study

The Iberian Massif represents a well preserved fragment of the Variscan basement, allowing characterization of the most complete geotraverse through the Variscan Fold Belt in Europe (Ribeiro, 1981; Matte, 1986; Franke, 1989). It comprises different zones, as depicted in Fig. 1a, divided according to their lithostratigraphic and structural features, and bounded either by major tectonic contacts or narrow belts with distinctive geological characteristics (Lötze, 1945; Julivert et al., 1974, 1980; Farias et al., 1987; Franke, 2000). In this framework, the internal continental segment of the SW Iberian Variscides corresponds to the OMZ, placed between the CIZ, to the north, and the SPZ, to the south. Using the concept of *"Tectono-stratigraphic Terranes"* introduced by Coney et al. (1980), a somewhat different zoning for the SW Iberian Variscides emerges, as proposed by Quesada (1991). Here, the OMZ and CIZ form the Iberian Terrane which, to the south, is brought in contact with the South-Portuguese Terrane through two assembled exotic terranes known as the Beja-Acebuches Ophiolite Complex (BAOC) and the Pulo do Lobo Terrane (PLT).

2.1 Geological background

The OMZ includes an ancient core of Proterozoic age upon which different (volcano) sedimentary sequences were added, mostly during the Lower Paleozoic. Following the *"Tectono-stratigraphic Terrane"* perspective, two major stages of accretion were responsible for the present-day OMZ architecture (Quesada, 1991; Ribeiro et al., 2007). The first one, developed during Vendian (Upper Proterozoic) time, led to the formation of the Iberian Terrane and was crucial for the crustal arrangement at the OMZ northern boundary. The second stage, accomplished in the course of the Variscan Orogeny (but mainly throughout the oblique continental collision that occurred in Upper Devonian to Carboniferous), led to the juxtaposition of the OMZ with BAOC, PLT and SPZ terranes, playing a crucial role in the configuration of the OMZ southern boundary.

2.1.1 OMZ boundaries

The exact position of the northern limit of the OMZ is a controversial issue despite the abundance of data. For some authors it corresponds to the NW-SE igneous alignment known as the “Los Pedroches Axis” (e.g., Lötze, 1945; Julivert et al., 1974) – Fig. 1b. For other authors, it coincides with the Tomar-Badajoz-Córdoba shear belt (TBCS), even though with distinct geodynamic meaning: a Variscan suture (Matte, 2001; Simancas et al., 2001) or a Cadomian suture reworked in Upper Paleozoic times as an intra-plate sinistral flower structure (Ribeiro et al., 1990; 2007 ; Quesada, 1991; Ribeiro, 2000). The recent re-evaluation of stratigraphic and palaeogeographic data led San José et al. (2004) to the conclusion that this boundary does not correspond to a simple lineament. Instead, it represents a narrow WNW-ESE band (the Lusitan-Marianic Zone), with distinctive characteristics, bounded by a pre-Variscan structure (subsequently sealed by the Los Pedroches batholith forming the “Los Pedroches Axis”) to the north, and the Alter do Chão - Malcocinado Fault Zone, to the south.

The OMZ southern limit has not been significantly modified since Lötze (1945), although the actual significance of some geological units remains open to debate (Fig. 1b). Following the most widely accepted interpretation, this boundary is the only rooted Variscan suture in Iberia (Ribeiro, 1981; Munhá et al., 1989; Quesada et al., 1994; Díaz Aspiroz et al., 2004). In this context, the Exotic Terranes BAOC and PLT represent, respectively, an obducted (and tectonically dismembered) ophiolite suite and an oceanic accretionary wedge developed from Lower to Middle Devonian times (Araújo and Ribeiro, 1995; Fonseca et al., 1999; Ribeiro et al., 2007). The current contact between PLT and OMZ or BAOC and PLT corresponds to the Ferreira-Ficalho-Almonaster Thrust Zone, which is intersected and displaced by the ENE-WSW, sub-vertical Ficalho-Aroche strike-slip fault. However, accumulated evidence strongly suggests that the Ferreira-Ficalho-Almonaster Thrust Zone is merely a shallow expression of a re-activated, deeper and more complex structure developed in the course of the OMZ-SPZ late-collision stages (Mateus et al., 1999; Figueiras et al., 2002; Vieira da Silva et al., 2007).

2.1.2 OMZ internal architecture

The outcome of successive decades of multidisciplinary research supports the division of the OMZ into distinct belts (domains), the most widely accepted being the one reported in Apalategui et al. (1990) based on tectonic criteria (structural style and deformation age). This division consists of, from north to south, the Portalegre-Badajoz-Córdoba belt, the North-Central Belt, the South-Central Belt, and the Southern Crystalline Complexes (Fig. 1b). Despite several debatable issues concerning the lateral continuity and kinematics of some tectonic structures, it can be shown that the limits of these belts (domains) coincide with major thrust zones, roughly trending NW-SE and subjected to repeated re-activation in Variscan times (Ribeiro, 1981; Quesada, 1991; Araújo, 1995). Accordingly, it is plausible to admit that the geometry of these thrusts was strongly influenced by pre-existing fault zones, delimiting intra-continental basins of variable extent and depth (Oliveira et al., 1991; Quesada, 1991, Eguíluz et al., 2000, Silva and Pereira, 2004; Pereira et al., 2006a). Locally, these tectonic contacts are displaced by late, strike-slip fault zones, especially those running between NNE-SSW and NE-SW, such as the Messejana Fault Zone, and those oriented approximately ENE-WSW, such as the Ficalho-Aroche Fault. The Messejana Fault, an outstanding deep structure that can be followed for approximately 530 km, was initiated in Late-Variscan times but successively re-activated during the Alpine Orogeny, as documented both by multiple injections of dolerite rocks (Cebriá et al., 2003) and distinct displacements in geological formations of different ages.

2.1.3 Main lithostratigraphic features

The oldest outcropping rocks in the OMZ (Fig. 2) are meta-sediments and meta-volcanics of Neoproterozoic age, possibly deformed during Cadomian events and particularly well exposed in the Portalegre-Badajoz-Córdoba and North-Central belts, although they can form small windows in the southernmost OMZ domains (e.g. Eguíluz et al., 2000; Fernández-Suárez et al., 2000; Simancas et al., 2004). The Upper Vendian to Lower Cambrian sequences comprise felsic meta-volcanics and arkosic meta-sandstones, besides meta-conglomerate levels, passing up into thick Lower Cambrian successions typical of carbonate platform; these sequences are fairly well represented in the North-Central belt and in the SW compartment of the Southern Crystalline Complexes Belt. Monotonous piles of pelites and meta-greywackes with inter-bedded mafic volcanics represent the common sequences of Middle and Upper Cambrian age that are particularly well exposed in the North-Central and South-Central belts. The Lower Ordovician sequence is essentially made up of pelites passing up into Silurian quartzites that are overlain by a condensed shale sequence of Silurian-Early Devonian(?) age, that can be properly observed both in the North-Central and South-Central belts (Oliveira et al., 1991; Robardet and Gutiérrez-Marco, 2004). In the SW compartment of the Southern Crystalline Complexes Belt, the Cambrian-Ordovician-Silurian transitions are a subject of controversy because of the strong tectonic dismembering and stacking, and because of difficulties in dating accurately some key formations. Nevertheless, according to recent data (Araújo et al., 2005), the uppermost outcropping units in this belt are interpreted as tectonic *mélanges*. Meta-sedimentary sequences of Upper Devonian age, especially preserved in the South-Central belt, are thick and flyschoid in character, resting unconformably on older formations. Lower and Middle Carboniferous sequences, sometimes with coal beds, occupy limited areas currently interpreted as intra-mountain basins (Eguíluz et al., 2000; Wagner, 2004; Pereira et al., 2006b).

All of these lithostratigraphic sequences were subjected to Variscan deformation and metamorphism, being also intruded by different igneous bodies. Strain accommodation took place heterogeneously in the course of three main phases of deformation (D_1 at ≈ 370-360 Ma, D_2 at ≈ 340 ± 20 Ma, and D_3 at 310 ± 10 Ma), generating a large variety of structures that can be observed at all scales (e.g. Ribeiro et al., 2007; Quesada, 1991;Jesus et al., 2007). The early metamorphic event (≈ 370 Ma) is represented by eclogite / blueschist rocks preserved in several D_1 nappes to be found in the Southern Crystalline Complexes Belt (Moita et al., 2005a, b, c). The typical (regional) metamorphism recorded by the OMZ rocks progressed, however, under greenschist to amphibolite facies conditions and occurred during D_2 (Quesada and Munhá, 1990; Castro et al., 1999; López-Munguira and Nieto García, 2004). The igneous record is also multistage and compatible with these main geodynamic evolving stages; the available data allow us to distinguish bodies that represent magmatism triggered by subduction (≈ 360 Ma) from those generated and emplaced during and after the OMZ-SPZ oblique collision (from ≈ 355 Ma to ≈ 300 Ma), the latter documenting the early to post-collision igneous activity provided by different magmas (Castro et al., 1999; Pin et al., 1999; Salman, 2004; Ribeiro et al., 2007). Despite these different granitoids, it is worth noting the presence of Lower Paleozoic (≈ 470-460 Ma) intrusions that show effects of Variscan deformation and outcrop both in the Portalegre-Badajoz-Córdoba and North-Central belts (Simancas et al, 2004; Salman, 2004). Cenozoic (mainly clastic) sediments, forming sequences of variable thickness related to the evolution of both major river systems and restricted basins controlled by (still active) strike-slip fault zones, cover significant areas of the OMZ Proterozoic-Paleozoic basement.

2.2 Synopsis of previous electromagnetic imaging

From the geological features reported in the previous section, a moderate to high resistive behavior for the shallow crustal levels of OMZ is expected with two main possible exceptions. The first is the crustal domains, where the Upper Proterozoic sequences show graphite-rich meta-sediments. The second corresponds to major fault zones that, regardless of their geometry and kinematics, preserve sufficient quantities of interstitial aqueous fluids or are sealed by mineral infillings that might result in adequate electrical contrasts in relation to the host rocks. The results obtained from MT surveys carried out in SW Iberia (profiles S, P, O and L in Fig. 3) during the last decade confirmed this general prediction (Monteiro Santos et al. 1999, 2002; Almeida et al. 2001, 2005; Pous et al. 2004; Muñoz et al. 2005). However, they also provided evidence of other distinctive features, namely (i) the complex character at depth of the OMZ boundaries, and (ii) the presence of middle-crust conductors locally displaced by discrete sub-vertical bands or disrupted by resistive domains, interpreted as deep tectonic structures or resistive igneous bodies, respectively. Nevertheless, the images reported in those papers are insufficient to provide the desired regional view of the main geoelectrical structures in the OMZ. Indeed, the lateral extension and geometry of these geoelectrical structures, besides the spatial wideness of the detected conductive / resistive domains should be addressed. The work of Vieira da Silva et al. (2007), presenting a 3D model for the Portuguese part of the OMZ-SPZ boundary, shows that some debatable issues can be properly analyzed on this basis. The MT data currently available for the whole OMZ justifies the development of a comprehensive 3D electromagnetic model, thus helping the characterization of the OMZ deep crustal architecture and the OMZ boundaries at depth. Moreover, resolving the real extension of middle-crust conductors in the OMZ highlights the role of crustal heterogeneities in *décollement* tectonics related to the SW Iberian Variscides development, which can be compared with those often involved in the growth of common orogenic belts.

3. The new, integrative 3D model of the OMZ

The MT data acquired along the six profiles displayed in Fig. 3 were analyzed or re-analyzed. Previous publications discuss the data along the individual profiles: profile P (Monteiro Santos et al. 1999, Almeida et al. 2001), profile O (Pous et al. 2004), profile S (Almeida et al. 2005), and profile L (Muñoz et al. 2005). The resistivity structures along all of these profiles show a preferred strike direction between N100E – N125E and were interpreted assuming the structure was two-dimensional. The new MT data presented in this paper consist of profiles I and E. Profile I, located in the westernmost area of the OMZ, is a NNE trending 145 km long profile consisting of 24 sites (Fig. 3) and the short profile E is located between profiles S and P with the same orientation and consists of 6 sites. Figure 4a shows six representative sites from profile I (sites 21, 16, 3, 1, 10 and 12) and Figure 4b one site (6) from profile E (site 6). As was the case for the previous profiles, the new data were acquired within the 0.004 s to 4000 s period range. The measurement dipoles used to record the horizontal electric and magnetic fields were oriented geomagnetic N-S and E-W. The vertical magnetic field component was recorded at 15 sites on profile I and at 4 sites on profile E. Estimation of the impedance tensor and transfer functions were carried out by using robust processing techniques (Egbert and Booker, 1986). A dimensionality analysis of profile I was carried out by using the algorithm of McNeice and Jones (2001). This analysis showed a three-dimensional character of the data. Indeed, no consistent 2D strike direction could be found for a significant period range or group of sites, and the *twist* and *shear* curves show a frequency dependency at all strike directions. Figure 5 shows the induction vectors at three periods. Note that induction vectors (Parkinson convention) along profile I point to the West, indicating the presence of a conductive body to the west of the profile. As we will show below the behavior of the induction vectors cannot be explained by the effect of the ocean alone but also requires a highly conductive body beneath the Tejo basin. The shape of the sounding curves also suggests the presence of strong lateral conductivity changes adjacent to the profile. For example the apparent resistivities in Fig. 4a, the XY mode (X - north; Y- east) is descending at longer periods whereas the YX mode increases at these long periods. This feature of the sounding curve is explained by a lateral conductor located east or west of the profile, and the direction of the induction vectors indicates that this conductor is located to the west of the profile. This behavior is inconsistent with a 2D structure; accordingly, 3D modeling is required. The other profiles, even though they have a mainly 2D character, also show some 3D characteristics, i.e. the component of the induction arrows parallel to the strike (roughly E-W) is not insignificant at some sites. The complete database (old and new sites) consist of impedance tensors from 148 sites with periods ranging from 0.004 s to 4000 s, and geomagnetic transfer functions (tipper) recorded at 88 of these stations with the same period range.

Three-dimensional forward modeling is by nature complex, particularly if a fine mesh is required in order to resolve large conductivity contrasts in different regions. The OMZ is an excellent case study for this type of modeling because of the large number of geoelectrical structures evident from the previous 2D models and because of the proximity of the Atlantic Ocean.

The mesh (cell size and dimensions) was chosen as a compromise between structure resolution and computational limitations. Accordingly, although it was refined in the areas close to the shoreline to take into account the great resistivity contrast between land and sea and in the areas where conductive anomalies appear, a coarser grid mesh was used and only the relevant large regional structures are attempted to be imaged in the model.

The 3D forward algorithm of Mackie et al. (1993) with the modifications reported in Mackie and Booker (1999) was employed. The modeling code uses 2D extensions in the horizontal directions and a 1D extension beneath the base of the 3D model; it establishes a tangential magnetic field as a boundary condition.

3.1 Ocean effect

The influence of the ocean on the MT data was evaluated by comparing the observed responses with those calculated using a simplified 3D model that incorporates the ocean (0.3 Ω.m) and a 1D resistivity model to represent crust and mantle (Fig. 6). Modeling was performed taking into account the Iberian Peninsula shoreline and the approximate bathymetry of the Atlantic Ocean. A mesh of 80 x 80 x 50 cells was used for the modeling. Cell size within the Iberian Peninsula is about 5 to 10 km, reducing to ~ 2-4 km at the coast. In the z direction cell sizes had to be much smaller to achieve convergence, 25 m for cells closest to the surface. The 1D model of crust and mantle consists of three layers: a 100 Ωm 350 m thick layer, a 500 Ωm 35 km thick layer and a 5000 Ωm 420 km thick layer representing the resistive mantle underlain by a 10 Ωm substratum (Fig. 6). The mantle resistivity was chosen taking into account mantle resistivities obtained in similar contexts (e.g. Constable and Constable, 2004; Monteiro Santos et al., 2003; Olsen 1998; Xu et al.

2000) although the mantle resistivity was overestimated to emphasize the influence of the ocean mass on the MT data (high skin depth).

Figure 6 shows the induction vectors calculated using this simplified model of the SW Iberian Peninsula at periods of 20 s and 100 s. Since the land model is 1D, the induction vectors respond solely to the presence of the ocean mass. At a period of 20 s the oceanic influence is significant only at the southernmost sites. At a period of 100 s the effect caused by the ocean mass disturbs mainly sites placed along profiles I, S, and those positioned in the southern half of profiles P and O. At longer periods the induction vectors at all sites respond to changes induced by the conductive water mass of the Atlantic Ocean (west and south of the studied area).

Figure 7 compares the effect caused by the oceanic water mass on the apparent resistivity and phase curves at sites nearest the coast for each profile with a site distant from the ocean. Also shown are the responses of the 1D crust/mantle model. The differences in model response are largest for profiles I and S. The influence on apparent resistivity values starts at about 10 s, and at about 5 s for phases. The difference is greater in the XY (X- north; Y east) polarization for profiles I and S as the influence of the western oceanic water mass increases. For profiles P and O the difference is greater in the YX polarization (east-west current flow) because of the southern position occupied by the oceanic water mass. The oceanic effect reduces as the distance from the coast increases. At distances greater than 200 km (e.g. northernmost site of profile O) the effect of the ocean is negligible at our longest periods.

From this study one can conclude that the oceanic effect has two different components, one coming from the water mass located to the west and the other resulting from the water mass located to the south. The western component affects mainly sites from profiles I and S at periods longer than 100 s, except for the southernmost sites where the influence starts at 5-10 s. At longer periods ($T \approx 1000$ s) the western component affects the entire surveyed region. The southern component affects the southernmost sites from profiles O and P at periods longer than 10 s.

The measured induction vectors at the shortest periods ($T < 10$ s) in profile I have greater magnitudes than those calculated using the “ocean model” for the same periods; consequently, the influence of the oceanic water alone cannot be invoked to explain this behavior. This result was useful in the 3D model building of the OMZ, because it indicates that a shallow conductor is required to the west of profile I. The long induction arrows measured at the southernmost sites in profiles P and O can neither be explained by the Atlantic Ocean influence alone, suggesting the presence of a shallow conductive anomaly to the south of both profiles.

3.2 Three-dimensional model of the OMZ

A selection of the most representative sites for imaging the regional structure was made on the basis of the morphology of their apparent resistivity and phase curves. Thus, all the apparent resistivity curves were grouped into zones, each of which had curves of similar morphology, which coincided with major geological units. From each group, one or more sites were selected to complete the database for 3D modeling. Thus, the MT data used consisted of the apparent resistivity and phase curves for 61 chosen sites and the geomagnetic transfer functions (tipper) for 55 of these sites (the sites selected are marked in red in Fig. 3). This site selection had the added benefit of reducing the effect of local galvanic distortion (although not that at regional-scale, if present) on the data given that by choosing morphologies that are common to a group of sites a regional pattern weakly affected by local distortions should be achieved. The scattering in the levels of the apparent resistivities was not greater than one decade and the levels of the curves were shifted to an average level for each group, so that the apparent resistivity values at short periods were the same. These values generally are similar to the resistivity values obtained from 2D inversions from previous data.

The starting model was built using the conductivity distribution obtained from the 2D models and the induction vector data (Fig. 5) as guides. The induction vectors help position conductive regions outside the area of data coverage, the vectors pointing to (Parkinson convention) high conductivity regions. A mesh was built starting with a horizontal cell size of about 5 km in the central part of the model. Tests were then carried out using finer meshes in both horizontal and vertical directions until the calculated responses were asymptotically stable. The greatest source of instability was found to be the vertical size of the cells. To further assure the suitability of the discretization, a section across the 3D model was chosen for 2D modeling. The corresponding 3D responses were then compared with the 2D responses calculated with the code of Wannamaker et al. (1987) and using a similar mesh size for the 3D model (see e.g. Queralt et al. 2007). The agreement of the 2D and 3D responses gives further confidence that discretization effects are negligible. The mesh used for the modeling consists of 80 (N-S) x 77 (E-W) x 76 (vertical) cells. The average cell size employed was 4 x 4 km in the horizontal plane. In the vertical directions the cell size increases approximately exponentially from 25 m in the first layers beneath the surface, 100 m at 1 km depth, 400 m at 5 km depth, and so on to 50 km depth where the cell height reaches 5 km. Below 45 km, where the deepest resistivity structures were located, several layers of uniform conductivity were used in order to assure the uniformity of the electric field at the base of the 3D core of the model. The whole model occupies a volume of 737 x 763 x 85 km, fully covering the OMZ and their boundaries.

After eighty-four 3D forward models, a feasible fit was obtained (Figs. 9, 10). The model sought to fit the apparent resistivity and phase curves of the off-diagonal components of the impedance tensor. In addition, the real and imaginary parts of both components of the geomagnetic transfer functions were fit. For the westernmost sites (profile I), the diagonal components of the MT impedance tensor were also fit. Figure 4 shows the data and model responses for some representative sites. The forward modeling provides a good insight into the resolution of the geoelectrical structures that possibly exist and allows us to identify those structures that are required by the data. During the modeling procedure the location, extent and resistivity value of the different structures were changed to assess the sensitivity of the model to the data. Special emphasis was placed on the structures of most significance for the geological interpretation.

Despite the complexity of the model and the difficulties in fitting diagonal components of the impedance tensor, a reasonable fit was achieved. The RMS of the misfit for periods between 0.1 s and 3000 s and for each kind of data was calculated assuming an error floor of 10% for the apparent resistivities, 5º for the phases and 0.05 for the magnetic transfer functions. The global RMS is 5.42 for the apparent resistivities of the off-diagonal components, 2.79 for the phases of the off-diagonal components, 14.96 for the apparent resistivities of the diagonal components (profile I only) and 2.86 for the magnetic transfer functions. The overall RMS misfit for all the data is 4.58 The fit is distributed almost uniformly in the whole area as can be seen for example in Fig. 8 where the absolute difference between observed and calculated phases along the MT profiles are shown. In general, phase differences are less than 10º for intermediate and lower frequencies (except profile O); the misfit being greater for the highest frequencies which no attempt was made to fit in detail.

The final three-dimensional model differs most from the starting model for the off-profile features. The continuity of the different conductive and resistive structures was thoroughly tested to determine the robustness of the features. For example, while conductor C3 (associated with the SPZ/OMZ suture) must be continuous between the profiles O and P, the conductor cannot be continued between profiles P and S without producing a significant misfit with the data. In a similar way the interruptions in conductors C4, C5 and C8 (associated with the OMZ/CIZ suture) and conductor C9 (the conductive layer spanning the whole OMZ) were tested and found to be necessary in order to fit the data. These features are compatible with the resistivity distribution found in the 2D inversions of the different profiles. Figure 11 compares the responses of the final model (Figs. 9, 10) with some of the test models. In the first test (Fig. 11a) the resistive interruption of conductor C3 (associated with the SPZ/OMZ suture) and the southernmost part of profile S was removed. As can be seen in the responses of the southernmost sites of profile S (e.g. site S9 in the figure) the minima in the apparent resistivities become much deeper and thus do not fit the data. A second test (Figs. 11b and 11c) consisted in replacing the complex conductive structure formed by conductors C4, C5, C8 (associated with the OMZ/CIZ suture) and C9 (the conductive layer spanning the whole OMZ) by a simple layer with a resistivity of 20 Ωm from a depth of 10 km down to a depth of 30 km. In this case the complex structure is necessary to explain the splitting of the apparent resistivity curves (e.g. at sites P34 and O24 in the figure). In addition, the removal of the resistivity interruptions in these conductors yields deeper minima and thus increased misfit with the data. In another test (Fig. 11d) the localized conductor C6 was replaced by a more extended, less conductive feature. As shown in the figure, the misfit becomes much larger, the splitting of the apparent resistivities being due to the proximity of site E6 to the edge of conductor C6. By contrast, in the sensitivity test, this edge is located at some distance from site E6.

3.3 Resistivity distribution

The 3D resistivity model results for the OMZ show 9 distinct areas with high to moderate conductivity (C1 to C9) and three highly resistive areas (R1, R2 and R3) (Figs. 9, 10). At the surface, the most noteworthy feature corresponds to a moderately conductive domain (C1) that is NE-SW elongated and shows an "L" shaped tail to the southeast; its presence is essentially indicated by the western component of the induction arrows of profile I and the particular shape of apparent resistivities and phases (see Fig. 4a). Down to 10 km depth, C1 forms a well defined NNE-SSW conductive band ≈ 200 km long and 50-75 km wide, with a resistivity of 20 Ωm. The band becomes more conductive (10 Ωm) at deeper levels, but is less distinct below 15 km depth. In the north, C1 completely disappears below 20 km depth; its southern portion, however, can be followed to a depth of 30 km.

The conductive domain C2 is required to explain the induction vectors of the southernmost sites in profiles P and O. It can be followed down to 20 km depth, suggesting a progressive rotation from NE-SW to E-W and showing a gradual conductivity decrease with depth (1-5 Ωm in the first 3 km and 10 Ωm in the next 17 km).

C3 is a well-defined conductor (5 Ωm) that is resolved from 5 to 30 km depth and, in its maximum extent, runs for more than 180 km along the E-W direction, therefore representing the most important geoelectrical structure in the southern part of the surveyed area. The eastern segment of C3 is clearly defined at 5 km depth and dips to the west, showing a bent geometry that persists down to a depth of 30 km. The complete extension of C3 is only achieved after 15-20 km depth, when its western segment is clearly evident without any ambiguity.

C4, C5, C6 and C7 are clearly identified from 5 km depth downwards. These domains in the northern part of the surveyed area show similar directions (varying from WNW-ESE to NW-SE) and resistivity values (1 to 10 Ωm); their extent ranging between 50 and 200 km. From 10 to 15 km depth all these domains, including C8, enlarge and band together, merging into a wide middle-crust conductive layer, C9, which reaches a depth of 30 km (Fig. 9).

The image obtained also shows several high to very-high resistive domains (more than 2000 Ωm). R1 and R2 are the largest and most significant crustal resistive domains that represent typical features of the northern part of the surveyed area. R1 extends from 5 to 45 km depth and shows a kink geometry, between the conductors C5 and C7/C8 and limited to the east by C4; its resistivity is 5000 Ωm or greater. The R2 domain, also present at all depths, in the NW corner of the surveyed area is notably enlarged when C1 is reduced to its southern portion (below 20 km depth); its resistivity is at least 2000 Ωm. The R3 domain can be followed down to a depth of 20 km and shows a consistent positioning right from the surface level, sitting between C2 and C3.

Despite the coarseness of the grid used in this large model and the wide spatial sampling, the resulting model is consistent with that obtained in earlier 2D and 3D models (Monteiro Santos et al. 1999; Almeida et al. 2001, 2005; Pous et al. 2004; Muñoz et al. 2005; Vieira da Silva et al., 2007). The presence of these conductors was well established in the previous 2D models. Namely, C7 and C4 in profile L (Muñoz et al., 2005), C5, C6, C7 and C3 in profile O (Pous et al 2004), C2, C3, C6, C8 and C5 in profile P (Almeida et al. 2001) and C6 in profile S (Almeida et al., 2005). The contribution of our 3D modeling is the delineation of the resistivity structure for the new profile I and the confirmation of the lateral continuity of the main structures across the OMZ identified by previous 2D modeling. The merging of the main conductive anomalies in OMZ led to the image of one conductive layer spanning the whole OMZ and extending into the CIZ. This allows us to correlate the MT data acquired in different sampling profiles and, consequently, to visualize the resistivity pattern of the OMZ.

4. Geological interpretation

A reasonable geological interpretation of the resistivity patterns obtained should consider the resistivity contrasts produced by the spatial arrangement of diverse rock types that may contact each other tectonically. Given the spatial sampling (site and profiles distance) and the cells dimension used, only the geoelectrical structures with regional influence can be identified, sometimes integrating the response of close-spaced geological formations or sub-parallel, although distinct, tectonic structures. Accordingly, the conductive and resistive domains provided by the reported 3D model should reflect the main geological features at depth, thereby helping to solve pending issues regarding the nature and structure of the crust of the OMZ and along its western, southern and northern boundaries.

The geological significance of C1 is uncertain. At shallow depths C1 coincides with a part of the western Cenozoic sedimentary basin. However, the maximum thickness of the Cenozoic sedimentary sequence is ≈ 600 m and occurs in narrow NE-SW trending grabens, according to gravimetry, geoelectrical surveys and several drill-holes (Oliveira et al., 2001). Therefore, a more realistic interpretation is needed because C1 extends down to a depth of 30 km, preserving the NNE-SSW direction despite the strong disruption at about 15 km depth and the gradual vanishing of its northern portion. Considering these features together with the available geological data, it seems that, in the upper 10 km, C1 could represent the bulk resistivity of PLT and SPZ upper crust located to the west of the NNW-SSE thrust fault zone that currently makes up the OMZ western limit. Consequently, this tectonic boundary does not have any intrinsic feature that enables its resolution. Moreover, the conductivity increase in C1 from ≈ 15 km depth downwards may be taken as evidence for the presence of a different crustal layer at that depth. In this interpretative scenario C1 correlates with C2, their horizontal (and vertical?) separation being accomplished by an early NE-SW tectonic structure, subsequently re-activated by the Messejana fault zone in Late-Variscan times, as already reported by the work of Vieira da Silva et al. (2007) in the same area. Note also that the disruption of C1 at ≈ 15 km depth strongly suggests the presence of a sub-parallel tectonic structure to the north of the Messejana alignment. Nevertheless, this interpretation implies the need for a suitable explanation for both the moderate resistive behavior of these tectonic structures and for the C2 conductivity change with depth.

The weak resistivity contrast shown by the NE-SW deep tectonic structures could be explained by either or both the poor model resolution and the presence of the igneous roots of the outcropping dolerites. Variations in C2 conductivity are more complex and are believed to reflect different causes. The high conductivity of the uppermost part of C2 shows mainly the abundant massive sulphide bodies within the outcropping volcano-sedimentary successions that characterize the Iberian Pyrite Belt in SPZ, in addition to the presence of graphite-rich schists locally over-thickened as a result of the thin-skinned tectonic regime during Variscan times (e.g. Ribeiro and Silva, 1983; Oliveira, 1990; Quesada, 1998; Oliveira et al., 2004). From 5 to ≈ 15 km depth, the C2 spatial positioning and orientation strongly suggest that it corresponds to the remaining Upper Paleozoic sequences in SPZ. The higher conductivity of C2 compared to C1 at this depth range is interpreted as the strengthening of the bulk effect associated with the tectonically imbricate Upper Paleozoic complex (down to 8-9 km) and its contact with the Lower Paleozoic successions through a major *décollement* already evidenced by deep seismic profiles (Prodehl et al., 1975). From 15 to 20 km, the conductivity of C2 and

C1 is similar, representing the autochthonous Lower Paleozoic layer, in good agreement with the seismic data (Prodehl et al., 1975). As a result, the 20-30 km depth layer should mostly correspond to the SPZ lower crust (granulitic basement?), which is also consistent with the available seismic data (Prodehl et al., 1975). The R2-C1 (C2) electrical resistivity contrast suggests that the disruption of C1 at ≈ 15 km depth caused a significant rising of the C1 northern portion, thus allowing the spatial coexistence of different levels of the SPZ basement, the lower ones having a tendency to be more resistive.

The foremost geoelectrical structure identified by the 3D model is determined by the enlargement and coalescence of different upper to middle-crust conductive domains in OMZ, quite obvious at ≈ 15-20 km depth, but continuing down to ≈ 30 km (C9, Fig. 9). At a depth of 20 km this sub-horizontal structure covers more than 200 km in E-W direction and almost 185 km in a N-S direction, merging the internal conductive domains with those related with the OMZ boundaries (such as C3 and C8 – see below). It thus represents a middle-lower crustal level that, in the first 5 km (roughly from 15 to 20 km depth), behaves as a sole conductive layer locally interrupted by plutonic intrusions (like R1) and/or displaced by deep, sub-vertical tectonic structures (such as C6). The electromagnetic imaging obtained is compatible with a granulitic basement that extends as far as the Moho transition (≈ 30-35 km depth, also pointed out by Simancas et al., 2003, using seismic data) and is thought to comprise a variable fraction of interconnected grain-boundary films of graphite (Monteiro Santos et al., 2002). The conductivity is higher at the top of this layer and that feature can result from a more effective connectivity of graphite at this level (15-20 km). This is emphasized when results of a recent seismic profile are considered (Simancas et al., 2003; Carbonell et al., 2004), showing that a straight spatial correspondence exists between the conductive layer and a 2 s thick reflective band, known as Iberian Reflective Body (IRB).

The most promulgated interpretation of IRB considers this huge band as a large layered igneous sill, presumably the source of Lower Carboniferous magmas (Simancas et al., 2003; Carbonell et al. 2004; Tornos and Chiaradia, 2004; Tornos and Casquet, 2005; Tornos et al., 2005). However, as noted by Pous et al. (2004), the presence of this igneous sill should produce a resistive rather than conductive behavior, unless a multiple sheet-like intrusion separated by screens of graphite-bearing metamorphic rocks is considered. For this reason, a significant part of the ≈ 15-20 km depth layer was interpreted as the base of a Proterozoic meta-sedimentary pile (Pous et al., 2004); even so, only a fortuitous convergence of causes might justify the presence of a deep metamorphic level consistently enriched in graphite and almost uniformly distributed all over the OMZ. Further considerations regarding either the constraints imposed to multiphase magma emplacement in a (very) special rheological crust level or the thermal regimes suitable for a long-lived and widespread magma feeding led Vieira da Silva et al. (2007) to favor the alternative interpretation already drawn in Monteiro Santos et al. (2002) and Almeida et al. (2005). The conductive and reflective layer IRB should represent not an igneous sill but a very important middle-crust *décollement*, largely developed immediately above or coinciding with the top of the OMZ granulitic basement. A very recent review concerning the abundance and timing of the early to post-collisional Variscan magmatism in OMZ also supports this alternative interpretation (Jesus et al., 2007). Therefore, the development of a wide conductive layer in OMZ at a depth of ≈ 15-20 km could be caused by a reinforcement of the conductive behavior resulting from the formation of graphite fine-aggregates along movement planes related to this major *décollement*. Additionally, domains of the *décollement* that are intersected by very deep sub-vertical tectonic structures or act as “merging points” of fault zones recognized at shallower crustal levels are potential sites for the development of massive graphite aggregates provided that Crich fluids were generated and their circulation sufficiently effective. In these circumstances, some sort of electrical anisotropy can be developed nearby or within the conductive layer, tending to form a sequence of blobs of higher conductivity (Heise and Pous, 2001, 2003).

As stated above, limits of the OMZ internal belts coincide with major thrust zones, consistently trending NW-SE and often subjected to several re-activation events. Some of these tectonic structures are resolved in the 3D electromagnetic imaging now obtained despite the general moderate to high resistive character in the first 5 km depth (see below). Of these, the boundaries between belts that constitute the northern part of the OMZ stand out, as shown in Fig. 1b. It is worth noting that the deep conductor C6 roughly divides the OMZ into two blocks, of distinct electrical behavior, with depths down to 10 km. Another prominent feature concerns the fact that all these tectonic structures show a distinctive conductive character from 8 to ≈ 20 km depth, reaching a maximum contrast (and differentiation, although preserving their trend) at a depth of 15 km, the top of the middle-crust *décollement*.

The difficulty of resolving the tectonic limits between the OMZ internal belts along the initial 8 km depth is interpreted as a consequence of the abundant igneous bodies currently existing at shallow crustal levels regardless of the problems caused by the coarse mesh used in the model construction. That is why the average electrical structure is moderately to highly resistive (500-2000 Ωm), allowing in spite of this the delimitation of highly resistive zones (5000 Ωm). The shallowest are easily correlated with the roots of prominent outcropping granitoid batholiths or gabbro-diorite complexes that developed during the Variscan orogeny (e.g. Carretero et al., 1990; Pin et al., 1999; Salman, 2004; Jesus et al., 2007). Note, however, that from 8 km downwards, only two main resistive domains persist. The first one, labeled R1, extends down to 45 km depth and may reflect the crustal distribution of different igneous rocks related to the deep magmatic activity that developed continuously in Paleozoic times roughly along the OMZ and CIZ boundary. The second one (R3) cannot be traced below 20 km depth, but shows a consistent positioning right from the surface level, sitting between C2 and C3; it should also represent variable outputs of the Variscan magmatic activity, roughly located along the PLT and SPZ boundary.

The electromagnetic imaging obtained does not shed much light on the debate on the real position of the OMZ-CIZ boundary. It simply reveals that there is a very good correspondence between the trace of the major, graphite bearing, tectonic structures that organize the crust in this complex belt and a group of sub-parallel deep conductors (C8-C7, C4 and C5), which show a tendency to merge in the western domain at a depth of ≈ 20 km (Fig. 9). However, an alternative interpretation may be considered. In fact, the relative positioning of these conductors at different depths strongly suggests that C8 is sub-vertical. Accordingly, C8 is the only geoelectrical structure that may represent the OMZ-CIZ boundary, clearly defined down to 27 km depth and reflecting the bulk signal of TBCS, which includes different sub-parallel thrust zones. This NW-SE conductor extends for more than 220 km and, in the easternmost domain of the surveyed area, merges with C7 (a shallower conductive anomaly whose top is evidenced at a depth of 6 km), reflecting suitably the geometric pattern of the main outcropping tectonic structures (Fig. 1b). From this perspective, C4 and C5 are envisaged as important features of the CIZ southern border, perhaps tracing the development of thrust systems that start to merge at 10 km depth. The gradual coalescence of C4 and C5 form a middle-crust conductive layer that joins the one recognized in the OMZ and extending into CIZ. At greater depths, however, C4 and C5 are still detected, thereby suggesting that their electrical properties are due to causes similar to those aforementioned for OMZ. The merit of this alternative interpretation resides in its good agreement with the seismic data reported in Simancas et al (2003) and Carbonell et al. (2004), which indicated the continuity of the IRB into the CIZ.

The OMZ southern boundary roughly coincides with C3, an elongated geoelectrical structure that strikes approximately E-W and can be followed for more than 180 km. The whole extension of C3 can only be appreciated from 15 to 30 km depth, despite a small break in its westernmost portion caused by the early NE-SW tectonic structure related to the C1-C2 separation. In the top 5 km, C3 is not detected; instead, a transition between two resistive domains comes into view, reflecting a slight contrast in the bulk electrical conductivity between geological formations belonging to the OMZ southern border and to PLT-BAOC-SPZ. The first conclusive evidence of C3 emerges at a depth of 5 km, revealing a bent structure that is confined to the easternmost segment of the geological contact, perhaps integrating the influence of different tectonic structures, such as early thrust zones along the Variscan suture affected by the ENE-WSW, sub-vertical Ficalho-Aroche strike-slip fault (Fig. 1b). The top of the remaining portion of C3 becomes visible only at 15 km depth; this is consistent with the results reported in Vieira da Silva et al. (2007) that allowed settling the roots of BAOC (made up of resistive rocks) from 12 km depth onwards. Accordingly, the westernmost portion of C3 shows a weak contrast with C2 between 15 and 20 km depth, given their spatial proximity and the local tectonic disturbance, which becomes clearly resolved at deepest levels (> 22 km) where it should really trace the Variscan suture. This interpretative background is consistent with other geological evidence that strongly supports either the late character of the Ferreira-Ficalho-Almonaster Thrust Zone (Mateus et al., 1999; Figueiras et al., 2002), or significant differences in the suture geometry reflecting primary dissimilarities on the OMZ-SPZ tectonic boundary (e.g. Quesada et al., 1994; Fonseca, 1995; Fonseca et al., 1999; Díaz Aspiróz et al., 2004; Jesus et al., 2007; Ribeiro et al., 2007).

5. Implications for *décollement* tectonics

The new 3D electromagnetic image obtained for OMZ and its boundaries provide evidence of an extensive middle to lower crustal conductive layer (≈ 15 to 30-35 km depth), its top (≈ 15-20 km depth) being of higher conductivity, already corroborated by previous studies (Monteiro Santos et al. 2002; Almeida et al. 2001, 2005; Pous et al. 2004; Muñoz et al. 2005). This top is interpreted as a major *décollement* between the granulitic basement and the overlying meta-sedimentary pile. The geotectonic units sited to the north and south of OMZ (CIZ and SPZ, respectively) seem to develop an identical sub-horizontal structure at similar depth, although poorly resolved given the extent of the MT profiles and parameterization used in model building. The same deduction was reported in earlier works that exploited just part of the MT data used in this study (Monteiro Santos et al., 1999; Muñoz et al., 2005; Vieira da Silva et al, 2007). At the OMZ-CIZ boundary (e.g. Ribeiro, 1981, 2000; Quesada, 1991; Ribeiro et al., 1990, 2007; Simancas et al., 2001, 2004) the two middle-crust *décollements* merge, even though the trace of the main geoelectrical structures can be followed from 20 km depth onwards as far as the Moho transition (at a depth of 30-35 km). A somewhat distinct framework develops at the OMZ-SPZ boundary (e.g. Munhá et al., 1989; Quesada et al., 1994; Araújo, 1995; Fonseca, 1995; Fonseca et al., 1999; Diaz Aspiroz et al., 2004). This is, in part, due to significant (and possibly primary) differences between the eastern and western segments of the tectonic boundary, currently separated by a Late-Variscan, ENE-WSW strike-slip fault. However, the influence caused by the tectonically complex belt that includes the Exotic Terranes PLT and BAOC cannot be ignored, particularly along the first 10-15 km depth. The whole extension of the SW Iberian Variscan suture is resolved without ambiguity from 22 km to 30 km depth, where the transition to the Moho should occur. From this brief statement, it seems that *décollement* tectonics played a crucial role in stress and strain partition within the lithosphere during the SW Iberian Variscides development, agreeing with geological inferences as discussed by, e.g., Matte (1986, 2001), Franke (2000) and Ribeiro et al. (2007). Accepting this interpretation, which is in good agreement with the available seismic reflection data (Simancas et al., 2003; Carbonell et al., 2004), two main questions may be posed: (1) what kind of crustal heterogeneities were mainly involved in the *décollement* tectonics and how were they generated?; (2) what were the major rheological and thermal constraints involved in the SW Iberian Variscides development? Answering these questions not only helps to understand better this Paleozoic Orogen, but also raises some questions about the issues concerning the growth of common orogenic belts.

The common rheological stratification shown by the continental lithosphere reflects its strength variation with depth (recording mostly changes on mineral composition, fluid abundance and temperature), even though the rate, duration and style of the accommodated deformation ultimately depend on the uppermost mantle layer strength (England and Mckenzie, 1982; Houseman and England, 1986; Ranalli and Murphy, 1987; Grocott et al., 2004). These interdependent relationships strongly influence the pattern of vertical (stress and) strain partitioning during the orogenesis in which the shallow and more deformed crustal level is decoupled from the lower crust, which in turn is decoupled from the uppermost mantle, by *décollement* systems (e.g. Cook, 1984; Oldow et al., 1990; Tikoff et al., 2004). Therefore, taking into account the geodynamic evolution experienced by the OMZ (e.g. Ribeiro et al., 2007) and the results of different numerical modeling (Harry et al., 1995; Teyssier and Cruz, 2004), sub-horizontal shear zones (acting as *décollements* and transmitting the shear stress) are expected to develop in the lower and middle crust as a natural consequence of contraction in a rheologically stratified lithosphere (Beaumont and Quilan, 1994; Harry et al., 1995). However, given the discrepancy between the geodynamic evolution experienced by the northern and southern OMZ boundaries, some particular features must be considered.

Assuming that the OMZ northern boundary represents a Cadomian suture re-activated during Variscan orogeny (e.g. Ribeiro, 1981; Matte, 1986, 2001; Ribeiro et al., 1990, 2007) implies the recognition of the pre-existence of an important crustal weakness, which determines strain partitioning in this crustal domain. In these circumstances, the development of a *décollement* at the base of the weak meta-sedimentary pile is favored, promoting vertical strain decoupling instead of pure shear thickening of the upper crust. Thus, in the underlying crystalline crust the magnitude of maximum strain decreases downward as strain becomes distributed over a wider area (Harry et al., 1995; Teysser and Cruz, 2004). Consequently, at all depths high strain accumulation will be restricted to the width of the region surrounding the weakened portion of the lithosphere, with the locus of highest strain resting near the TBCS inner belt. This will favor the development of sub-parallel thrust zones that tend to merge in a sole *décollement*, as observed, separating the tectonically disrupted upper crust from the relatively un-deformed crystalline basement. Further evolution will therefore be strongly influenced by the generated mechanical heterogeneities at middle crustal or shallower depths.

The development of the OMZ overall conductive and reflective middle-crust layers should be related to the mechanical heterogeneities generated during the OMZ-SPZ continental collision, namely throughout the formation of a kinematically coupled system that incorporates a pro-wedge (the Iberian Pyrite Belt in SPZ), an axial zone (PLT) and a retro-wedge (the OMZ southernmost belt) domain (Jesus et al., 2007). Indeed, the presence of an important foreland basin in the SW Iberian Variscides strongly suggests that crustal thickening during orogenic shortening impeded the creation of a large crustal root, and excess buoyancy within the lithosphere resulting in a very limited uplift of the shallow crust, as corroborated by numerical models (Harry et al., 1995). This statement is also compatible with the fact that basal foreland thrusts are not rooted beneath the hinterland, and that (thin-skinned) deformation in the foreland is restricted to the upper 10 to 15 km of the crust, as deduced from the available seismic reflection profiles. Accordingly, the foreland shortening could not be accommodated within the OMZ hinterland by homogeneous contraction, favoring crust decoupling from the underlying mantle and re-enforcing the thermal weakness character of the OMZ southern border (acting as a retro-wedge system); this mechanical behavior was further assisted by significant magmatism as a result of the local incursion of the asthenospheric mantle allowed by the inferred slab break-off (Jesus et al., 2007).

Following the results of numerical and analogue models (e.g. Harry et al., 1995; Tikoff et al., 2004; Willingshofer et al., 2005), the crust-upper mantle decoupling in OMZ during the early collision stages should be represented by a *décollement* deforming at a high rate of high strain, which could extend beneath the entire width of the hinterland, causing contraction and local thickening of the lower crustal level. Concurrently, pure shear shortening and crustal thickening is expected to progress in the upper crust of the OMZ southern border. The outstanding geological record of the structures that reflect this strain accommodation is consistent with the development of a second *décollement* at the base of the weak meta-sedimentary pile in the middle crust, partially decoupling strain in the lower crust from strain within the upper crust.

As collision proceeds, deformation at middle-crust and shallower depths on the OMZ southern border would be more concentrated where the middle-crust *décollement* is straining most quickly. Therefore, deformation in the upper crust of the OMZ southern border should be driven by shear along the middle-crust *décollement*, which is expected to be less rapid and more broadly distributed than on the BAOC, PLT and SPZ northern boundary. In subsequent geodynamic stages, the middle-crust *décollement* should have been able to widen, expanding toward the OMZ interior and allowing the propagation of deformation in the upper crust toward the hinterland. Consequently, the thrust systems observed in OMZ only penetrate to middle-crust levels, leaving the lower crust un-faulted, thereby supporting the interpretation for the IRB and the top of the conductive layer. This general inference is also compatible with the available geological data that enable us to deduce several hundreds of kilometers of shortening over a period of 90-100 Ma, providing additional evidence of multiple orogenic episodes over periods of several tens of Ma (e.g. Ribeiro et al., 2007).

The conformity existing between MT and seismic surveys for OMZ and SPZ, as well as their agreement with geological interpretations based on detailed mapping and multidisciplinary research, strongly suggests that major *décollements* developed at middle and lower-crustal depths play a crucial role in orogen growth. These *décollements* extend throughout the entire width of the orogen and provide a successively increasing degree of decoupling between deformation in the shallow crust and deeper levels. This significant strain partitioning within the lithosphere, is believed to be a common feature of orogens involving oblique continental collision (Sanderson and Marchini, 1984; Oldow et al., 1990, Teyssier et al., 2002; Grocott et al., 2004).

6. Conclusions

Earlier MT surveys on OMZ have elucidated a number of resistive and conductive features that are related to major structural features and play a significant role in the architecture of this terrane. The 3D electromagnetic imaging now obtained, covering entirely the OMZ and its boundaries, corroborates earlier results and, for the first time, provides a complete picture of the geometry and wholesale spatial distribution of the detected resistivity pattern. A brief synthesis of the features resolved is given below:

(1) PLT and SPZ geological formations in contact with OMZ are more conductive than those belonging to the OMZ terrane along the upper 10 km depth.

(2) The NNW-SSE thrust fault zone that currently makes up the OMZ western limit has no intrinsic feature that enables its electrical resistivity resolution.

(3) The *décollement* inferred from seismic data for SPZ, splitting the upper thin-skinned complex from the Lower Paleozoic cover at ≈ 8-9 km depth, is not accurately resolved by MT data. Conversely, this latter crustal layer (15-20 km depth) and the top of the SPZ (granulitic?) basement show a conductive character that, probably, reflects the presence of interconnected graphite films in rock matrixes or that of graphite aggregates that fulfill movement planes associated with deep-seated *décollements*.

(4) The OMZ southern boundary roughly coincides with an elongated geoelectrical structure that strikes approximately E-W and can be followed for more than 180 km. The Variscan suture can only be completely resolved from ≈ 22 km depth onwards given the poor electrical resistivity contrasts obtained for upper crustal levels and the compositional / structural discrepancy along the OMZ-SPZ boundary.

(5) Some of the tectonic structures that bound the OMZ internal belts are resolved despite the general moderate to high resistive character showed by the crust in the first 5 km depth.

(6) The widespread conductive character of the OMZ crustal layer from ≈ 15 to 30-35 km depth is interpreted as a result of graphite distribution in the granulitic basement. The

higher conductivity of the upper part of this layer (≈ 15-20 km depth) should reflect mostly an important middle-crust *décollement* enriched in fluid-deposited graphite as a consequence of Variscan shearing.

(7) There is spatial correspondence between the major OMZ middle-crust *décollement* and the 2 s thick reflective band, known as the Iberian Reflective Body (IRB – Simancas et al., 2003; Carbonell et al., 2004).

(8) The main outcropping, sub-parallel thrust zones that form the OMZ-CIZ boundary, are evidenced by an important NW-SE conductor that extends for more than 220 km, and in the easternmost domain of the surveyed area merges with a shallower conductive anomaly.

(9) The thrust systems along the CIZ southern border also seem to be unraveled by two conductive structures that start to merge at ≈ 10 km depth and define a middle-crust conductive layer that joins the one recognized in OMZ.

Mechanical heterogeneities that may have influenced the deformation style in the SW Iberian Variscides result mainly from the geodynamic evolution experienced by the OMZ-SPZ tectonic boundary. Strain partitioning into shallow (thin-skinned) deformation in the foreland (SPZ) and deep-seated deformation in the hinterland (OMZ) was primarily accommodated by the development of *décollement* systems in the middle and lower crusts which extend beneath the entire width of the orogen. The lateral growth of these *décollement* systems during shortening results both in the SPZ leading edge migration toward OMZ and in the gradual propagation of deformation to deeper crustal levels of the proximal foreland. Strain partitioning into deep-seated deformation in OMZ and shallow deformation in SPZ, and the progressive growth of deformation both outward and downward with time, are compatible with geodynamic models proposed for the SW Iberian Variscides that regard the OMZ southern boundary as the only rooted Variscan suture, and its northern boundary as a Cadomian suture re-activated in Variscan times.

Acknowledgements

This research was supported by the Spanish Ministry of Science project CGL2006-12259, the Consolider-Ingenio 2010 program, under CSD2006-00041 "Topo-Iberia" and by Acciones Integradas Hispano-Portuguesas. Critical comments from Alan Jones, Ian Fergusson, Philip Wannamaker and an anonymous reviewer contributed significantly to clarify the ideas presented in this paper and are deeply acknowledged.

References

Almeida, E., J. Pous, F. Monteiro Santos, P. Fonseca, A. Marcuello, P. Queralt, R. Nolasco, and L. Mendes Victor (2001), Electromagnetic imaging of a transpressional tectonics in SW Iberia, *Geophys. Res. Lett.*, 28, 439-442**.**

Almeida, E., F. Monteiro Santos, A. Mateus, W. Heise, and J. Pous (2005), Magnetotelluric measurements in SW Iberia: new data for the Variscan crustal structures analyses, *Geophys. Res. Lett.*,32, L08312, doi: 10.1029/2005GL022596.

Apalategui, O., L. Eguiluz and C. Quesada (1990), Structure, in *Pre-Mesozoic Geology of Iberia*, edited by R.D. Dallmeyer and E. Martinez-Garcia, pp. 280-291, Springer-Verlag, Berlin.

Araújo, A. (1995), Estrutura de uma geotransversal entre Brinches e Mourão (Zona de Ossa-Morena). Implicações na evolução geodinâmica da margem sudoeste do Terreno Atóctone Ibérico, *PhD Thesis*, Univ. Évora, Évora, Portugal.

Araújo, A. and A. Ribeiro (1995), Tangential transpressive strain regime in the Évora-Aracena Domain (Ossa Morena Zone), *Bol. Geol. y Minero*, 106, 111-117

Araújo, A., P. Fonseca, J. Munhá, P. Moita, J. Pedro and A. Ribeiro (2005), The Moura Phyllonitic Complex: an accretionary complex related with obduction in the Southern Iberia Variscan Suture, *Geodin. Acta*, 18/5, 375-388.

Avdeev, D.B. (2005), Three-dimensional electromagnetic modeling and inversion from theory to application, *Surv. Geophysics*, 26, 767-799.

Beaumont, C. and G. Quilam (1994), A geodynamic framework for interpreting crustal-scale seismic-reflectivity patterns in compressional orogens, *Geophys. J. Intern.*, 116, 754-783.

Carbonell, R., F., Simancas, C. Juhlin, J. Pous, A. Pérez-Estaún, F. González-Lodeiro, G. Muñoz, W. Heise, and P. Ayarza (2004), Geophysical evidence of a mantle derived intrusion in SW Iberia, *Geophys. Res. Lett.*, 31, L11601 doi:10.1029/2004GL019684.

Carretero, R.S., L. Eguíluz, E. Pascual and M. Carracedo (1990), Igneous rocks in *Pre-Mesozoic Geology of Iberia*, edited by R.D. Dallmeyer and E. Martinez-Garcia, pp. 292-313, Springer-Verlag, Berlin.

Castro, A., C. Fernández, H. El-Himdi, M. El-Biad, M. Díaz, J.D. De la Rosa and F. Stuart F. (1999), Age constraints to the relationships between magmatism, metamorphism and tectonism in the Aracena metamorphic Belt, Southern Spain, *Intern. Journ. Earth Sci.*, 88, 26-37.

Cebriá, J.M., J. López-Ruiz, M. Doblas, L.T. Martins and J. Munhá (2003), Geochemistry of the Early Jurassic Messejana-Placencia dyke (Portugal – Spain); implications on the origin of the Central Atlantic Magmatic Province, *J. Petrol.*, 44, 547-568.

Coney, P., D.L. Jones and J.W.H. Monger (1980), Cordilleran suspect terranes, *Nature*, 288, 329-333.

Constable, S. and C. Constable (2004), Observing geomagnetic induction in magnetic satellite measurements and associated implications for mantle conductivity, *Geochem. Geophys. Geosyst.*, 5, Q01006, doi:10.1029/2003GC000634.

Cook, F. (1984), Geophysical anomalies along strike of the southern Appalachian piedmont. *Tectonics*, 3, 45-62.

Díaz Aspiroz, M., A. Castro, C. Fernández, S. López, J.C. Fernández Caliani and I. Moreno-Ventas (2004), The contact between the Ossa Morena and the South Portuguese zones. Characteristics and significance of the Aracena metamorphic belt in its central sector between Aroche and Aracena (Huelva), *Journal of Iberian Geology*, 30, 25-51.

Egbert, G. and J.R. Booker, (1986), Robust estimation of geomagnetic transfer functions, *Geophys. J. R. Astron. Soc.* 87,173-194.

Egbert, G. and J.R. Booker (1992), Very long period magnetotellurics at Tucson observatory, *J. Geophys. Res.*, 97, 3397-3404.

Eguíluz, L., J.I. Gil Ibarguchi, B. Ábalos and A. Apraiz (2000), Superposed Hercynican and Cadomian orogenic cycles in the Ossa-Morena Zone and related areas of the Iberian Massif, *GSA Bulletin*, 112 (9), 1398-1413.

Eisel, M. and V. Haak. (1999), Macro-anisotropy of the electrical conductivity of the crust: a magnetotelluric study of the German Continental Deep Drilling Site (KTB), *Geophys. J. Int.*, 136, 109-122.

England, P., and D. McKenzie (1982), A thin viscous sheet model for continental deformation, *Geophys. J. R. astr. Soc.*, 70, 295-321.

Evans, S., A.G. Jones, J. Spratt and J. Katsube (2005), Central Baffin electromagnetic experiment (CBEX) maps the NACP in the Canadian arctic, *Phys. Earth Planet. Int.*, 150, 107-122.

Farias, P., G. Gallastegui, F. González Lodeiro, J. Marquínez, L.M. Martín Parra, J.R. Martínez Catalán, J.G. Pablo Macia and L.R. Rodríguez Fernández (1987), Aportaciones al conocimiento de la litoestratigrafia y estructura de Galicia Central. *Mem. Fac. Ciências Univ. Porto*, 1, 411-431.

Fernández-Suaréz, G., G. Gutiérrez Alonso, G. Jener, and M. N. Tubrett (2000), New ideas on the Proterozoic-Early Paleozoic evolution of NW Iberia: insights from U-Pb detrital zircon ages, *Precambrian Res.*, 102, 185-206.

Figueiras, J., A. Mateus, M. A. Gonçalves, J. C. Waerenborgh, and P. Fonseca (2002), Geodynamic evolution of the South Variscan Iberian Suture as recorded by mineral transformations, *Geodin. Acta*, 15, 45-61.

Fonseca P. (1995), Estudo da sutura Varisca no SW Ibério nas regiões de Serpa-Beja-Torrão e Alvito-Viana do Alentejo, *PhD Thesis,* Univ. Lisboa, Lisboa, Portugal.

Fonseca, P., J. Munhá, J. Pedro, F. Rosas, P. Moita, A. Araújo, and N. Leal (1999), Variscan ophiolites and high-pressure metamorphism in Southern Iberian, *Ophioliti*, 24, 259-268

Franke, W. (1989), Tectonostratigraphic units ins the Variscan belt of Central Europe, in *Terranes in the Circum-Atlantic Paleozoic Orogens, Special Papers*, vol. 230, edited by R. D. Dallmeyer, pp. 67-90, Geological Society of America.

Franke, W. (2000), The mid-European segment of the Variscides: tectonostratigraphic units, terrane boundaries and plate tectonic evolution, in *Orogenic Processes: quantification and modeling, Variscan Belt*, *Spec. Publ.* vol.179, edited by W. Frank, V. Haak, O. Oncken and D. Tanner, pp. 35-64, Geol. Soc. London.

Grocott, J., K.J.W. McCaffrey, G.K. Taylor and B. Tikoff (2004), Vertical coupling and decoupling in the lithosphere, in *Vertical Coupling and Decoupling in the Lithosphere, Special Publications*, vol. 227, edited by J. Grocott, K.J.W. McCaffrey, G.K. Taylor and B. Tikoff, pp. 1-7, Geological Society, London.

Harry, D.L., J.S. Oldow and D.S. Sawyer (1995), The growth of orogenic belts and the role of crustal heterogeneities in decollement tectonics, *Geol Soc. Amer. Bull.*, 107, 1411-1426.

Heise, W. and J. Pous (2001), Effects of anisotropy on the two-dimensional inversion procedure, *Geophys. J. Int.,* 147, 610-621.

Heise, W. and J. Pous (2003), The anisotropic modeling of phase anomalies exceeding 90º: A field data application, *Geophys. J. Int.*, 155, 308-318.

Hoffman-Rothe, A., O. Ritter and V. Haak (2001**),** Magnetotelluric and geomagnetic modeling reveals zones of very high electrical conductivity in the upper crust of Central Java, *Physics of the Earth Int*., 124, 131-151.

Houseman, G. and P. England (1986), Finite strain calculations of continental deformation, 1, method and general results for convergent zones, *J. Geophys. Res.*, 91, 3621-3663.

Jesus, A., J. Munhá, A. Mateus, C. Tassinari and A. P. Nutman (2007), The Beja Layered Gabbroic Sequence (Ossa Morena Zone, Southern Portugal): geochronology and geodynamic implications, *Geodin. Acta*, 20/3, 139-157.

Jones, A. (1998), Waves of future: Superior inferences from collocated seismic and electromagnetic experiments, *Tectonophysics,* 286, 273-298.

Jones, A.G., T.J. Katsube and P. Schwann (1997), The longest conductivity anomaly in the world explained: sulphides in fold hinges causing very high electrical anisotropy. *J. Geomag. Geoelectr.*, 49, 1619-1629.

Julivert, M., J.M. Fontboté, A. Ribeiro and L.S. Conde (1974), *Mapa Tectónico de la Península Ibérica y Baleares a escala 1:1.000.000*. IGME, Madrid.

Julivert M., F.J. Martínez and A. Ribeiro (1980), The Iberian segment of the European Hercynian Foldbelt, in *Géologie de l'Europ, Mémories du BRGM*, vol. 108, edited by J. Cogné and M. Slansky, pp. 132-158, Société Géologique du Nord / BRGM.

López-Munguira, A. and F. Nieto Garcia (2004), Low-grade metamorphism in the central sector of the Ossa-Morena Zone, *Journal of Iberian Geology*, 30, 109-118.

Lötze, F. (1945), Zur gliederung dês Variscides der Iberischen Meseta, *Geotektonische Forschungen*, 6, 78-92.

Mackie R.L. and T.R. Madden (1993), Three dimensional magnetotelluric inversion using conjugated gradient, *Geophys. J. Int.,* 115, 215-229.

Mackie, R.L. and J.R. Booker (1999), Documentation for mtd3fwd and d3-to-mt, GSY-USA, Inc., 226 Market St. 643, San Francisco, CA 94114.

Mackie, R.L., Madden, T.R. and P.E. Wannamaker (1993), Three-dimensional magnetotelluric modeling using difference equations - Theory and comparisons to integral equation solutions, *Geophysics*, 58, 215-226.

Mateus, A., J. Figueiras, M. A. Gonçalves, and P. Fonseca (1999), Evolving fluid circulation within the Variscan Beja-Acebuches Ophiolite Complex (SE, Portugal), *Ofioliti*, 24, 269-282

Matte, Ph. (1986), Tectonics and plate tectonics for the Variscan Fold Belt in Western Europe. *Tectonophysics*, 126, 329-374.

Matte, Ph. (2001), The Variscan collage and orogeny (480-290 Ma) and the tectonic definition of the Armorica microplate: a review, *Terra Nova*, 13, 122-128.

McNeice, G. and A. G. Jones (2001), Multisite, multifrequency tensor decomposition of magnetotelluric data, *Geophys*ics, 66, 158-173.

Moita P., J. Munhá, P. Fonseca, J. Pedro, C.C.G. Tassinari, A. Araújo and T. Palácios (2005a), Phase equilibria and geochronology of Ossa-Morena eclogites, paper presented at XIV Semana de Geoquímica / VIII Congresso de Geoquímica dos Países de Língua Portuguesa, Aveiro, Portugal, 463-466.

Moita P., J. Munhá, P. Fonseca, C.C.G. Tassinari, A. Araújo and T. Palácios (2005b), Dating orogenic events in Ossa-Morena Zone, paper presented at XIV Semana de Geoquímica / VIII Congresso de Geoquímica dos Países de Língua Portuguesa, Aveiro, Portugal, 459-461.

Moita P., J.F. Santos and M.F. Pereira (2005c), Dados geocronológicos de rochas intrusivas sin-tectónicas do Maciço dos Hospitais (Montemor-o-Novo, Zona de Ossa-Morena), paper presented at XIV Semana de Geoquímica / VIII Congresso de Geoquímica dos Países de Língua Portuguesa, Aveiro, Portugal, 471-474

Monteiro Santos, F.A., J. Pous, E.P. Almeida, P. Queralt, A. Marcuello, H. Matías and L. A. Mendes Victor (1999), Magnetotelluric survey of the electrical conductivity of the crust across the Ossa Morena Zone and South Portuguese Zone suture, *Tectonophysics*, 313, 449-462.

Monteiro Santos, F.A., A. Mateus, E.P. Almeida, J. Pous and L.A. Mendes-Victor (2002), Are some of the deep crustal conductive features found in SW Iberia caused by graphite?, *Earth Planet. Sci. Lett.*, 201, 353-367.

Monteiro Santos, F. A., A. Soares, R. Noslasco, H. Rodrigues, R. Luzio, N. Palshin and the ISO-3D team (2003), Lithosphere conductivity structure using the CAM-1 (Lisbon-Madeira) submarine cable, *Geophys. J. Int.,* 155, 591-600.

Munhá, J., A. Ribeiro, P. Fonseca, J.T. Oliveira, P. Castro and C. Quesada (1989), Accreted terranes in Southern Iberia: Beja-Acebuches ophiolite and related oceanic sequences, paper presented at 28th Int. Geol. Cong., Washington, U.S.A., 481-482.

Muñoz, G., W. Heise, C. Paz, E. Almeida, F. Monteiro Santos and J. Pous (2005), New magnetotelluric data trough the boundary between the Ossa Morena and Centroiberian Zones, *Geologica Acta*, 3, 215-223.

Oldow, J.S., A.W. Bally and H.G. Ave Lallemant (1990), Transpression, orogenic float and lithospheric balance, *Geology*, 18, 991-994.

Oliveira, J.T. (1990), Stratigraphy and syn-sedimentary tectonism in the South Portuguese Zone, in *Pre-Mesozoic Geology of Iberia*, edited by R.D. Dallmeyer and E. Martinez-Garcia, pp. 334-347, Springer-Verlag, Berlin.

Oliveira, J.T., V. Oliveira and J.M. Piçarra (1991), Traços gerais da evolução tectono-estratigráfica da Zona de Ossa-Morena, em Portugal, *Cuad. Lab. Xeológico de Laxe*, 16, 221-250.

Oliveira, V., J. Matos, C. Rosa (2001), The NNW sector of the Iberian Pyrite Belt – new exploration perspectives for the next decade, *in Massive Sulphide Deposits in the Iberian Pyrite Belt: New Advances and Comparison with Equivalent Systems*, *Proceedings of GEODE Workshop*, edited by F. Tornos, E. Pascual, R Saéz and R Hidalgo, pp. 34-37, Univ. Huelva, Aracena (Spain).

Oliveira, J.T., Z. Pereira, P. Carvalho, N. Pacheco and D. Korn (2004), Stratigraphy of the tectonically imbricated lithological succession of the Neves Corvo mine área, Iberian Pyrite Belt, Portugal, *Mineral. Deposita*, 39, 422-436.

Olsen, N. (1998), The electrical conductivity of the mantle beneath Europe derived from *C*-responses from 3 to 720 hr, *Geophys. J. Int.*, 133, 298–308.

Pereira, M.F., M. Chichorro, U. Linnemann, L. Eguíluz and J.B. Silva (2006a), Inherited arc signature in Ediacaran and Early Cambrian basins of the Ossa-Morena Zone (Iberian Massif, Portugal): paleogeographic link with European and North African Cadomian correlatives, *Precambrian Res.*, 144, 297-315.

Pereira, Z., V. Oliveira and J.T. Oliveira (2006b), Palynostratigraphy of the Toca da Moura and Cabrela Complexes, Ossa Morena Zone, Portugal. Geodynamic implications. *Rev. Palaeobot. Palynology*, 139, 227-240

Pin, C., J.-L. Paquette and P. Fonseca (1999), 350 Ma (U-Pb zircon) igneous emplacement age and Sr-Nd isotopic study of the Beja gabbroic complex (S. Portugal), paper presented at XV Reunion de Geologia del Oeste Peninsular, Diputación de Badajoz, Badajoz, Spain, 190-194.

Pous, J., G. Muñoz, W. Heise, J.C Melgarejo, and C. Quesada (2004), Electromagnetic imaging of Variscan crustal structures in SW Iberia: the role of interconnected graphite, *Earth Planet. Sci. Lett.*, 217, 435-450.

Prodehl, C., V.S. Moreira, St. Mueller and A.S. Mendes (1975), Deep-seismic sounding experiments in Central and Southern Portugal, paper presented at 14th General Assembly of the European Seismological Commission, Berlin, 261-266.

Queralt, P., A.G. Jones, and J. Ledo (2007), Electromagnetic imaging of a complex ore body: three-dimensional forward modelling, sensitivity tests and down-mine measurements, *Geophysics*, 72, 85-95.

Quesada, C. (1991), Geological constraints on the Paleozoic tectonic evolution of tectonostratigraphic terranes in the Iberian Massif, *Tectonophysics*, 185, 225-245.

Quesada, C. (1998), A reappraisal of the structure of the Spanish segment of the Iberian Pyrite Belt, *Mineral. Deposita*, 33, 31-44.

Quesada, C. and J. Munhá (1990), Metamorphism, in *Pre-Mesozoic Geology of Iberia*, edited by R.D. Dallmeyer and E. Martinez-Garcia, pp. 314-320, Springer-Verlag, Berlin.

Quesada, C., P. Fonseca, J. Munhá, J. T. Oliveira, and A. Ribeiro (1994), The Beja-Acebuches Ophiolite (Southern Iberian Variscan fold belt): geologic characterization and geodynamic significance, *Bol. Geol. Min.*, 105, 3-44.

Rannali, G. and D.C. Murphy (1987), Rheological stratification of the lithosphere, *Tectonophysics*, 132, 281-295.

Ribeiro, A. (1981), A geotransverse through the Variscan fold belt in Portugal, in *The Variscan Orogen in Europe*, *Geol. Mijnbouw*, vol. 60, edited by H.J. Zwart and V.F. Dornsiepen, pp. 41-44.

Ribeiro, A. (2000), Geodynamic evolution of Iberian Variscides: unsolved questions, in *Variscan-Appalachian dynamics: the building of the Upper Paleozoic basement*, paper presented at GALICIA 2000, Basement Tectonics 15, A Coruña, Spain.

Ribeiro A., J.B. Silva (1983), Structure of the South Portuguese Zone, in *The Carboniferous of Portugal*, *Mem. Serv. Geol. Portugal*, 29, edited by M.J. Lemos de Sousa and J. T. Oliveira, pp. 83-89.

Ribeiro A., C. Quesada and R.D. Dallmeyer (1990), Geodynamic evolution of the Iberian Massif, in *Pre-Mesozoic Geology of Iberia,* edited by R.D. Dallmeyer and E. Martinez-Garcia, pp. 397-410, Springer-Verlag, Berlin, Germany.

Ribeiro A., J. Munhá, R., Dias, A. Mateus, E. Pereira, L. Ribeiro, P. Fonseca, A. Araújo, J.T. Oliveira, J. Romão, H. Chaminé, C. Coke and J. Pedro (2007), Geodynamic evolution of the SW Europe Variscides, *Tectonics*, 26, doi:10.1029/2006TC002058.

Robardet, M. and J.C. Gutiérrez-Marco (2004), The Ordovician, Silurian and Devonian sedimentary rocks of the Ossa-Morena Zone (SW Iberian Peninsula, Spain), *Journal of Iberian Geology*, 30, 73-92.

Salman, K. (2004), The timing of the Cadomian and Variscan Cycles in the Ossa-Morena Zone, SW Iberia: granitic magmatism from subduction to extension, *Journal of Iberian Geology*, 30, 119-132.

San José, M.A., P. Herranz and A.P. Pieren (2004), A review of the Ossa-Morena and its limits. Implications for the definition of the Lusitan-Marianic Zone, *Journal of Iberian Geology*, 30, 7-22.

Sanderson, D. and R.D. Marchini (1984), Transpression, *J. Struct. Geol.*, 6, 449-458.

Sasaki, Y. (2004), Three-Dimensional Inversion for Large-Scale Structure in a Spherical Domain, *Earth Planet. Spaces*, 56, 239-248.

Silva, J.B. and M.F. Pereira (2004), Transcurrent continental tectonics model for the Ossa-Morena Zone Neoproterozoic-Paleozoic evolution, SW Iberian Massif, Portugal, *Int. J. Earth Sci.*, 93, 886-896.

Simancas, F., D. Martínez Poyatos, I. Expósito, A. Azor and F. González Lodeiro (2001), The structure of a major suture zone in the SW Iberian Massif: the Ossa-Morena/Central Iberia contact, *Tectonophysics,* 32, 295-308.

Simancas, F., R. Carbonell, F. González Lodeiro, A. Pérez Estaún, C. Juhlin, P. Ayarza, A. Kashubin, A. Azor, D. Martínez Poyatos, G.R. Almodóvar, E. Pascual, R. Sáez, and I. Expósito, (2003),The Crustal Structure of the Transpressional Variscan Orogen of SW Iberia: The IBERSEIS Deep Seismic Profile, *Tectonics*, 22(6), 1062, doi:10.1029/2002TC001479.

Simancas, F., I. Expósito, A. Azor, D. Martínez Poyatos and F. González Lodeiro (2004), From the Cadomian orogenesis to the Early Paleozoic Variscan rifting in Southwest Ibéria, *Journal of Iberian Geology*, 30, 53-72.

Simpson F. (2000), A three-dimensional electromagnetic model of the southern Kenya rift: departure from two dimensionality as a possible consequence of a rotating stress fields, *J. Geophys. Res.*, 105, 19321-19344.

Siripunvaraporn W., G. Egbert, Y. Lenbury and M. Uyeshima (2005), Three-Dimensional Magnetotelluric Inversion: Data Space Method, *Phys. Earth Planet. Int.*, 150, 3-14.

Tauber S., R. Banks, O. Ritter, U. Weckmann (2003), A high-resolution magnetotelluric survey of the Iapetus Suture Zone in southwest Scotland., *Geophys. J. Int.*, 153 , 548–568.

Teyssier, C. and L. Cruz (2004), Strain gradients in transpressional to transtensional attachment zones, in *Vertical Coupling and Decoupling in the Lithosphere*, *Geological Society*, *Special Publications*, vol. 227, edited by J. Grocott, K.J.W. McCaffrey, G.K. Taylor and B. Tikoff, pp. 101-115, London.

Teyssier, C., B. Tikoff and J. Weber (2002), Attachement between brittle and ductile crust at wrenching plate boundaries, in *Continental Collision and the Tecton-Sedimentary Evolution of Forelands, Special Publications,* vol. 1, edited by G. Bertotti, K. Schulmann and S. Cloetingh, pp. 57-73, European Geophysical Society.

Tikoff, B., R. Russo, C. Teyssier and A. Tommasi (2004), Mantle-driven deformation of orogenic zones and clutch tectonics, in *Vertical Coupling and Decoupling in the Lithosphere,* *Special Publications,* vol. 227, edited by J. Grocott, K.J.W. McCaffrey, G.K. Taylor and B. Tikoff, pp. 41-64, Geological Society, London.

Tornos, F. and C. Casquet C. (2005), A new scenario for the related IOCG and Ni-(Cu) mineralization: the relationship with giant mid-crustal mafic sills, Variscan Iberian Massif, *Terra Nova*, 17, 236-241.

Tornos, F., and M. Chiaradia (2004), Plumbotectonic evolution of the Ossa Morena Zone, Iberian Península: tracing the influence of mantle-crust interaction in ore-forming processes, *Econ. Geol.*, 99, 965-985

Tornos, F., C. Casquet and J.M.R.S. Relvas (2005), Transpressional tectonics, lower crust decoupling and intrusion of deep mafic sills: a model for the unusual metallogenesis of SW Iberia, *Ore Geology Reviews*, 27 (1-4), 133-163.

Varentsov, Iv. M., M. Engels, T. Korja, M. Smirnov, M. Yu. and the BEAR Working Group (2002), A generalised geoelectrical model of Fennoscandia: a challenging database for long-period 3D modellingstudies within the Baltic electromagnetic array research (BEAR) project. *Izvestiya, Physic of the Solid Earth*, 38, 11, 855-896.

Vieira da Silva, N., A. Mateus, F. A. Monteiro Santos, E. P. Almeida and J. Pous (2007), 3D electromagnetic imaging of a Paleozoic plate-tectonic boundary segment in SW Iberian Variscides (S Alentejo, Portugal), *Tectonophysics*, in press.

Wagner, R.H. (2004), The Iberian Massif: a Carboniferous assembly, *Journal of Iberian Geology*, 30, 93-108.

Wannamaker, P.E. (2000), Comment on 'The petrologic case for a dry lower crust' by B. W. D. Yardley and J. W. Valley, *J. Geophys. Res.*, 102, 6057-6064.

Wannamaker, P.E., Stodt, J.A and L.Rijo (1987), A stable finite element solution for two-dimensional magnetotelluirc modeling, *Geophys. Jour. Roy. Astro. Soc* , 88, 277-296.

Wannamaker, P.E., G.R. Jiracek, J.A. Stodt, T.G. Caldwell, V.M. Gonzalez, J.D. McKnight and A.D. Porter (2002), Fluid generation and pathways beneath an active compressional orogen, the New Zealand Southern Alps, inferred from magnetotelluric data. *J. Geophys. Res., 107*, doi:10.1029/2001JB000186.

Willingshofer E., D. Sokoutis and J.-P. Burg (2005), Lithospheric-scale analogue modeling of collision zones with a pre-existing weak zone, in *Deformation Mechanisms, Rheology and Tectonics: from Minerals to the Lithosphere*, *Special Publications*, vol. 243, edited by D. Gapais, J.-P. Burg and P.R. Cobbold, pp. 277-294, Geological Society, London.

Xu, Y., T. J. Shankland and B. T. Poe, (2000) Laboratory-based electrical conductivity in the Earth’s mantle, *J. Geophys. Res.*, 105(B12), 27865-27876, 10.1029/2000JB900299.

Figure Captions

Figure 1a – Main geotectonic units of the SW Iberia Variscides (adapted from Quesada, 1991). Grey-shaded area represents the Pre-Mesozoic basement in the Iberian Peninsula; CIZ – Central Iberian Zone; OMZ – Ossa Morena Zone; SPZ – South Portuguese Zone; PTZ – Porto-Tomar shear zone; TBCS – Tomar-Badajoz-Córdoba shear belt; ET – Exotic Terranes (PLT and BAOC, Pulo do Lobo Terrane and Beja-Acebuches Ophiolite Complex, respectively). Thick black lines represent the trace of the main tectonic boundaries with prevalent thrust or strike-slip displacement.

Figure 1b – OMZ belts (adapted from Simancas et al., 2004). 1- Messejana Fault; 2- Portalegre-Alegrete Thrust; 3- Hornachos-Villaharta Thrust; 4- Alter do Chão – Campo Maior Fault; 5- Azuaga Fault; 6- Malcocinado Fault; 7- Monesterio Thrust; 8- Juromenha Thrust; 9- Beja-Valdelarco Faul; 10- Ferreira Ficalho – Almonaster Thrust; 11- Ficalho-Aroche Fault

Figure 2 - Geological map of OMZ and its boundaries, resulting from an overview of current OMZ maps available in the Portuguese and Spanish Geological Surveys by using the same criteria, and plotting features with significance for the geological interpretation reported in the present paper. 1 – Cenozoic sedimentary cover; 2 – Odovician-Silurian to Carboniferous sequences in OMZ; 3 - Cambrian sequences in OMZ; 4 – Upper Proterozoic in OMZ; 5 – Paleozoic sequences in CIZ; 6 – Paleozoic sequences in SPZ [a) Phyllitic-Quartzitic Group, Upper Devonian; b) Volcanic-sedimentary Complex, Upper Devonian to Lower Visean; c) Flysh Group, Upper Visean to Lower Westfalian]; 7 – Exotic Terranes [a) Beja-Acebuches Ophiolite Complex; b) Pulo do Lobo Terrane]; 8 – Intrusive bodies (mostly granitic in nature and Variscan in age). Thin black lines represent the traces of the main tectonic discontinuities (thrust zones and strike-slip fault zones)

Figure 3 - Simplified geological map and location of the MT sites (dots). The red dots show the representative sites chosen for the 3D modelization. Legend as in figure 2.

Figure 4a - Data and model responses. Each row corresponds to one kind of data and each column to one site. Sites 21, 16, 3, 1, 10 and 12 of the new profile I.

Figure 4b - Data and model responses. Each row corresponds to one kind of data and each column to one site. Sites S09, S24, E06, P04, P34, O04, O19 and L10 (the first letter corresponds to the name of the profile).

Figure 5 - Real induction arrows (Parkinson convention) at 10, 100 and 1000 s.

Figure 6 - Plan view of the model used for the study of the ocean effect, including the bathymetry. The land part is represented by a 1D model (upper right panel). The induction arrows are shown in Parkinson convention at periods of 20 s and 100 s.

Figure 7 - Ocean effect in the apparent resistivity and phase curves for the sites closest to the sea at each profile and one site located far away from the ocean (marked with a star). The solid line represents the response of the 1D land model.

Figure 8 – Pseudo-sections of the absolute phase difference between data and model responses for all the profiles.

Figure 9 - 3D electrical resistivity model. Plan view at different depths. The black dots indicate the location of the MT sites used for the study. The shore line and the surface occurrence of the SPZ/OMZ and OMZ/CIZ sutures (see figures 2 and 3) are shown to facilitate the location of the structures.

Figure 9 (Cont.).

Figure 10 - Plan view of the model at a depth of 22 km and two cross sections along a NS profile and an EW profile (Vertical exaggeration = 2). The resistivity values have been grouped to highlight the most striking conductivity features. Conductors C1, C3 and C6 merge into the conductive layer C9. The black dots indicate the location of the MT sites. The shoreline and the surface occurrence of the sutures SPZ/OMZ and OMZ/CIZ (see figures 2 and 3) are shown to facilitate the location.

Figure 11 – Data and model responses for different sensitivity tests. The dots represent the data, the solid lines the responses of the final model (Figs. 9, 10) and the dashed lines the responses of the altered models: a) Without the resisitive interruption of conductor C3 in the south of profile S. b) and c) With a 20 Ωm layer spanning the whole OMZ from 10 to 30 km depth instead of the conductive structure of the final model. d) With conductor C6 replaced by a more extended 20 Ωm conductive body.

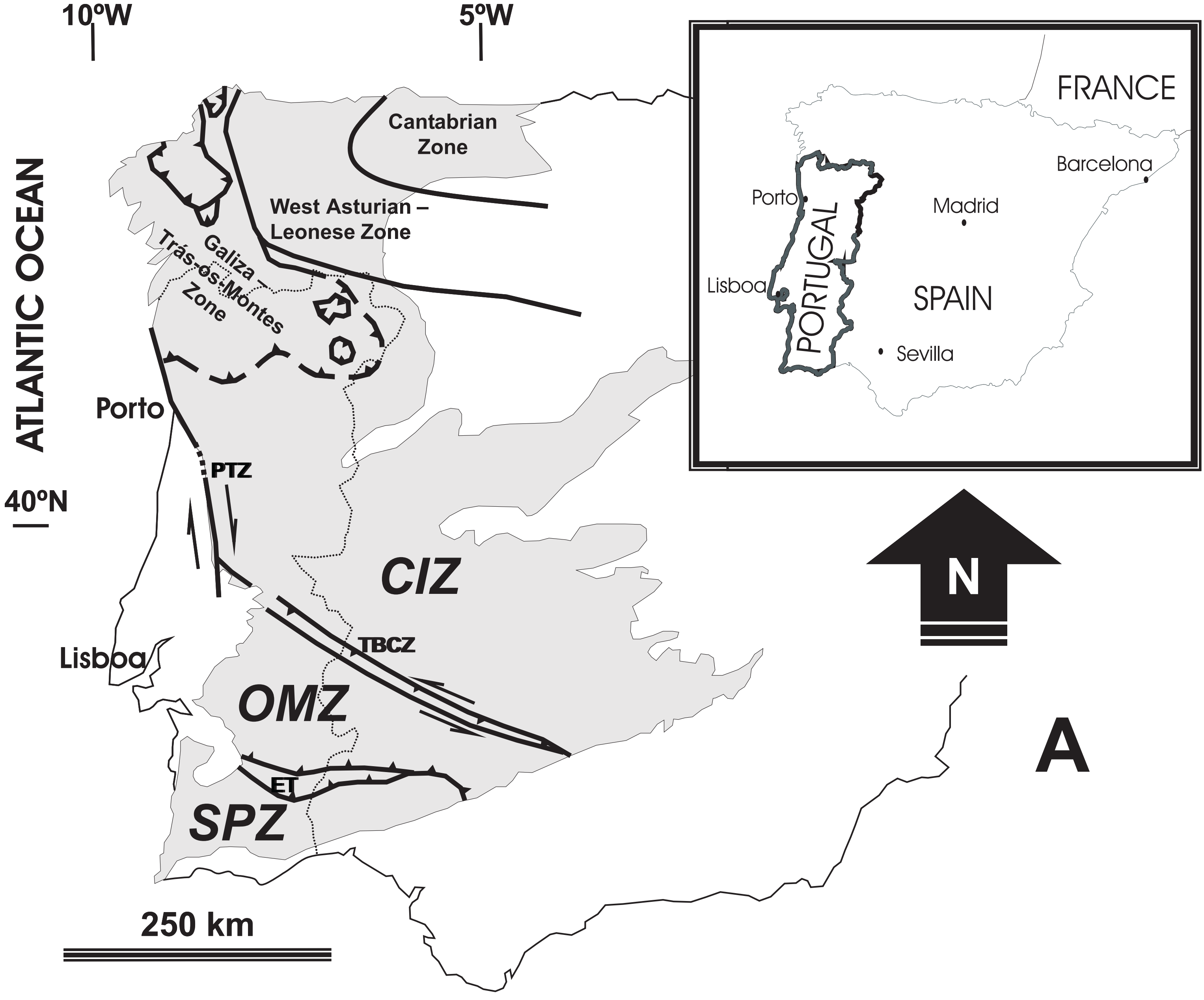

Figure 1a: Main geotectonic units of the SW Iberia Variscides (adapted from Quesada, 1991). Gray-shaded area represents the Pre-Mesozoic basement in the Iberian Peninsula; CIZ Central Iberian Zone; OMZ Ossa Morena Zone; SPZ South Portuguese Zone; PTZ Porto-Tomar shear zone; TBCS Tomar-Badajoz-Córdoba shear belt; ET Exotic Terranes (PLT and BAOC, Pulo do Lobo Terrane and Beja-Acebuches Ophiolite Complex, respectively). Thick black lines represent the trace of the main tectonic boundaries with prevalent thrust or strike-slip displacement.

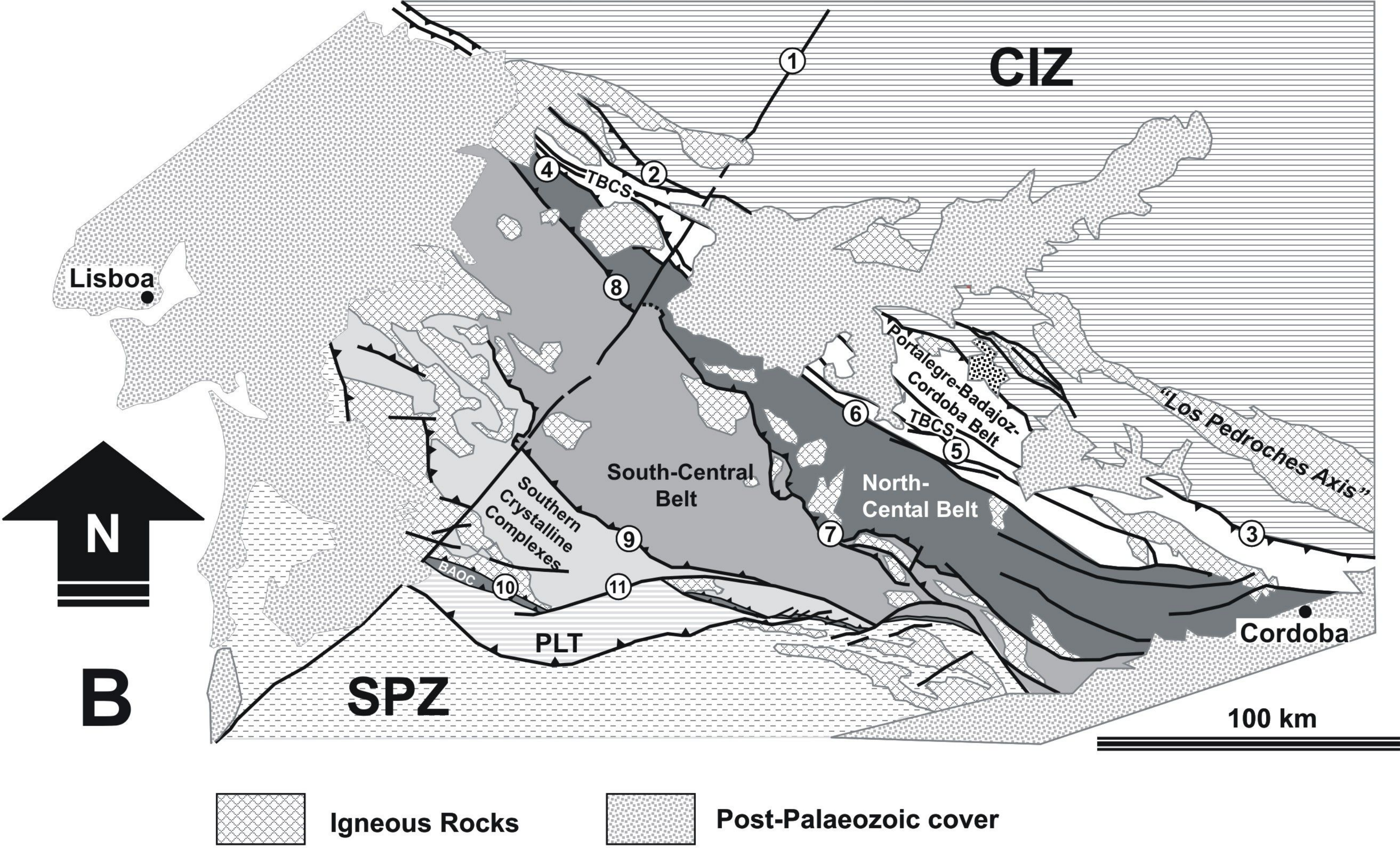

Figure 1b: OMZ belts (adapted from Simancas et al., 2004). 1- Messejana Fault; 2- Portalegre-Alegrete Thrust; 3- Hornachos-Villaharta Thrust; 4- Alter do Chão Campo Maior Fault; 5- Azuaga Fault; 6- Malcocinado Fault; 7- Monesterio Thrust; 8- Juromenha Thrust; 9- Beja-Valdelarco Fault; 10- Ferreira Ficalho Almonaster Thrust; 11- Ficalho-Aroche Fault.

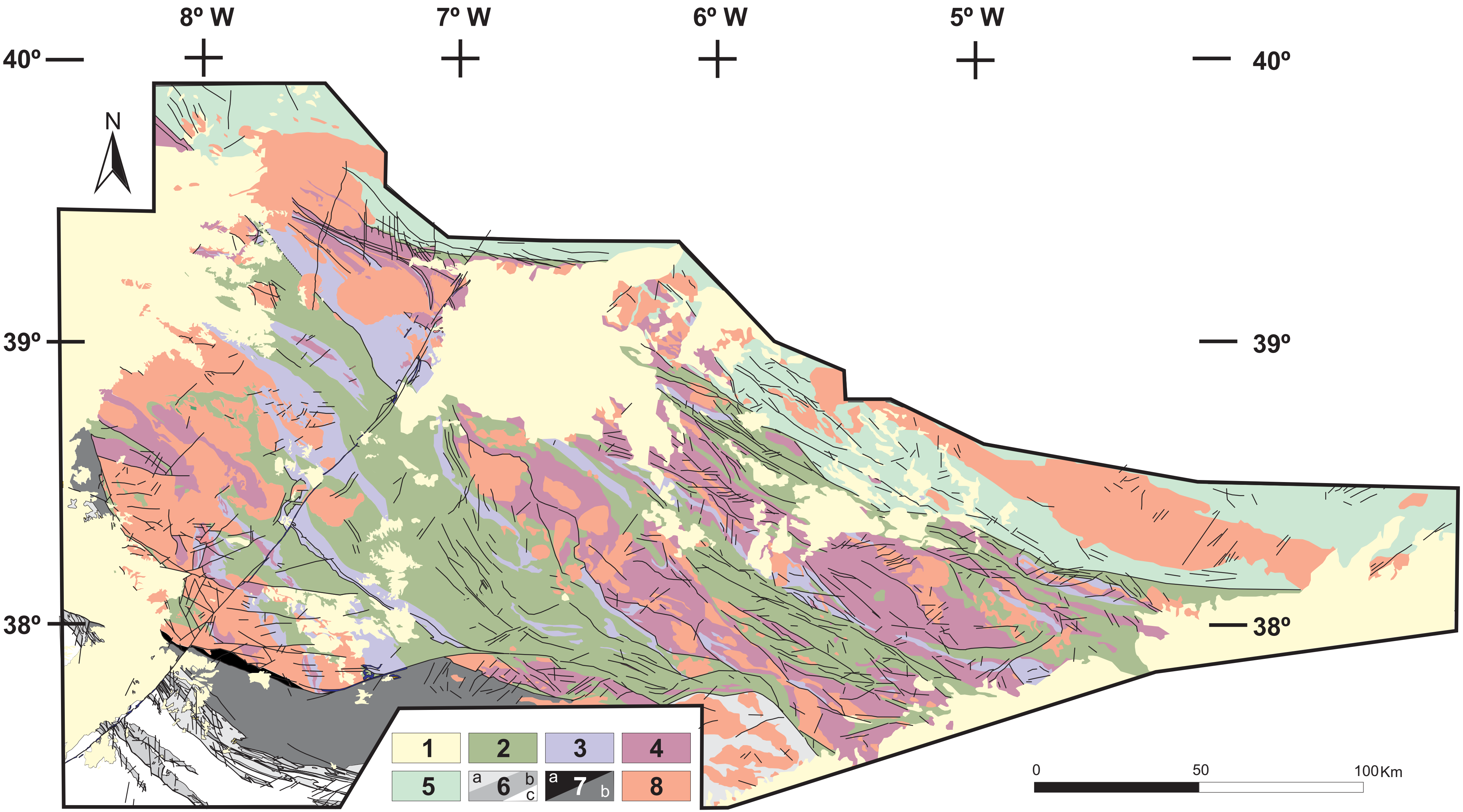

Figure 2: Geological map of OMZ and its boundaries, resulting from an overview of current OMZ maps available in the Portuguese and Spanish Geological Surveys by using the same criteria, and plotting features with significance for the geological interpretation reported in the present paper. 1- Cenozoic sedimentary cover; 2 - Odovician-Silurian to Carboniferous sequences in OMZ; 3 - Cambrian sequences in OMZ; 4 - Upper Proterozoic in OMZ; 5 - Palaeozoic sequences in CIZ; 6 - Paleozoic sequences in SPZ [a) Phyllitic-Quartzitic Group, Upper Devonian; b) Volcanic-sedimentary Complex, Upper Devonian to Lower Visean; c) Flysh Group, Upper Visean to Lower Westfalian]; 7- Exotic Terranes [a) Beja-Acebuches Ophiolite Complex; b) Pulo do Lobo Terrane]; 8 - Intrusive bodies (mostly granitic in nature and Variscan in age). Thin black lines represent the traces of the main tectonic discontinuities (thrust zones and strike-slip fault zones)

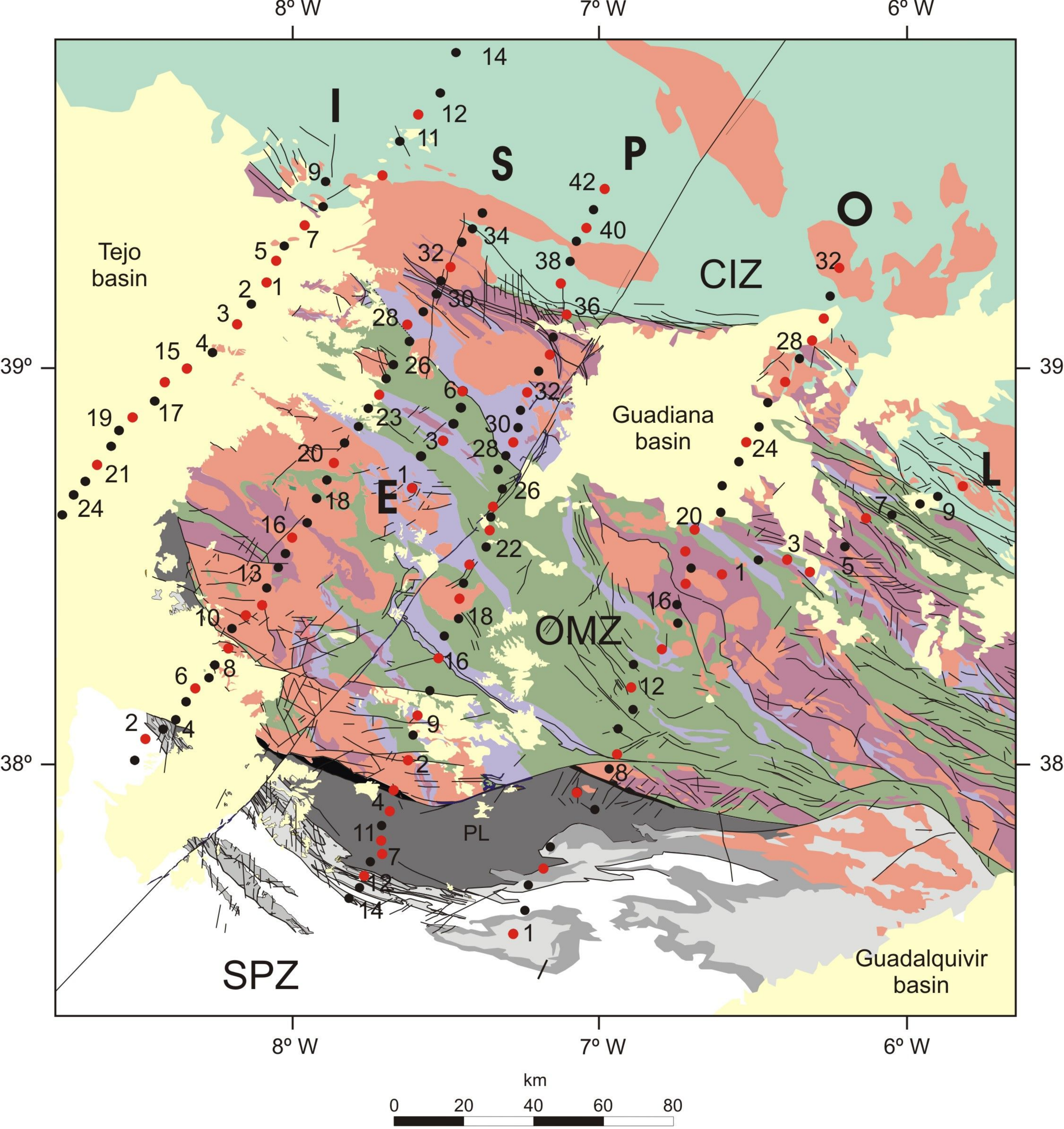

Figure 3. Simplified geological map and location of the MT sites (dots). The red dots show the representative sites chosen for the 3D modelization. Legend as in figure 2.

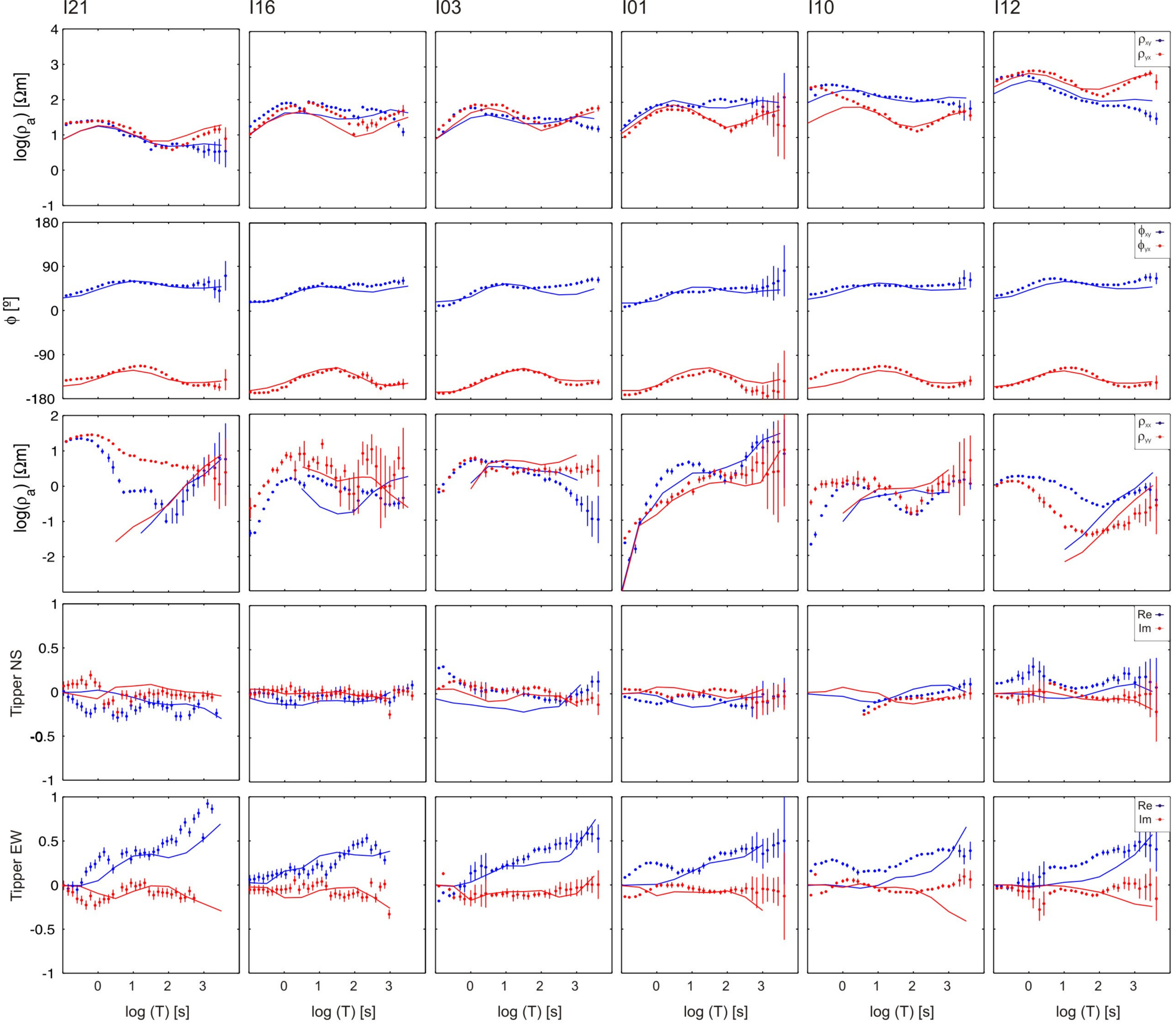

Figure 4a. Data and model responses. Each row corresponds to one kind of data and each column to one site. Sites 21,16,3,1,10 and 12 of the new profile I.

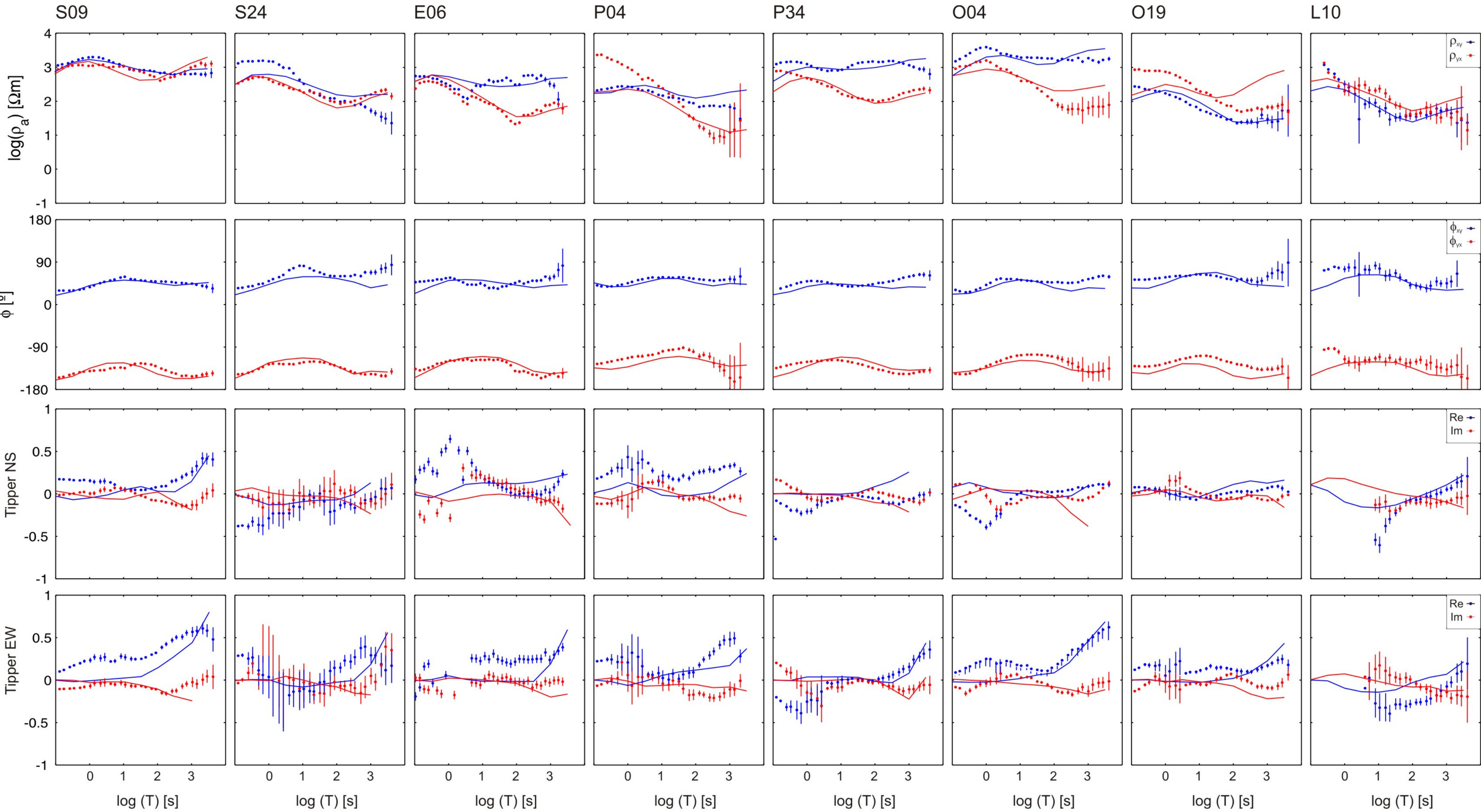

Figure 4b. Data and model responses. Each row corresponds to one kind of data and each column to one site. Sites S09, S24, E06, P04, P34, O04, O19 and L10 (the first letter corresponds to the name of the profile)

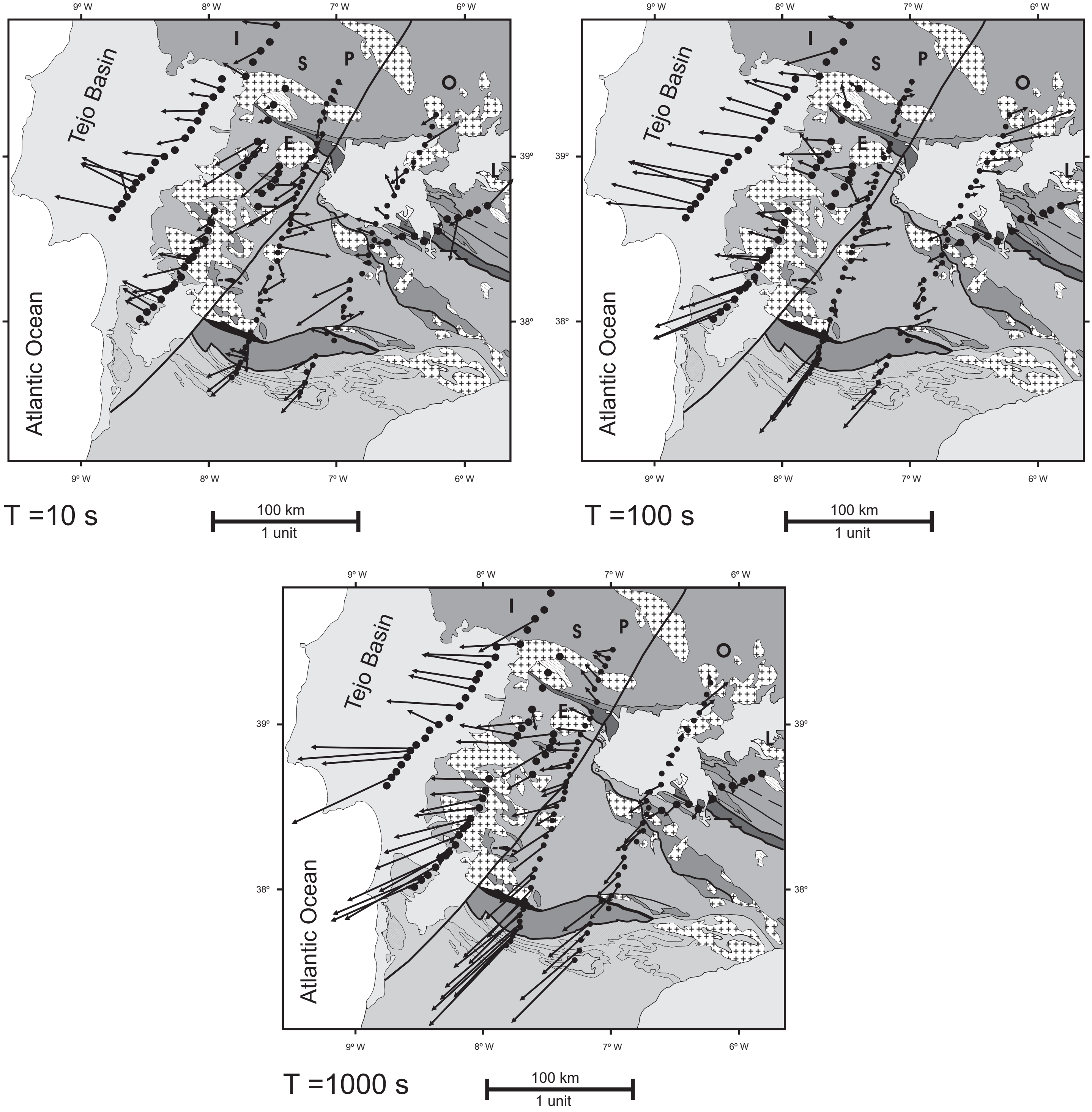
T =10 s

T =100 s

T =1000 s

Figure 5. Real induction arrows (Parkinson convention) at 10, 100 and 1000 s.

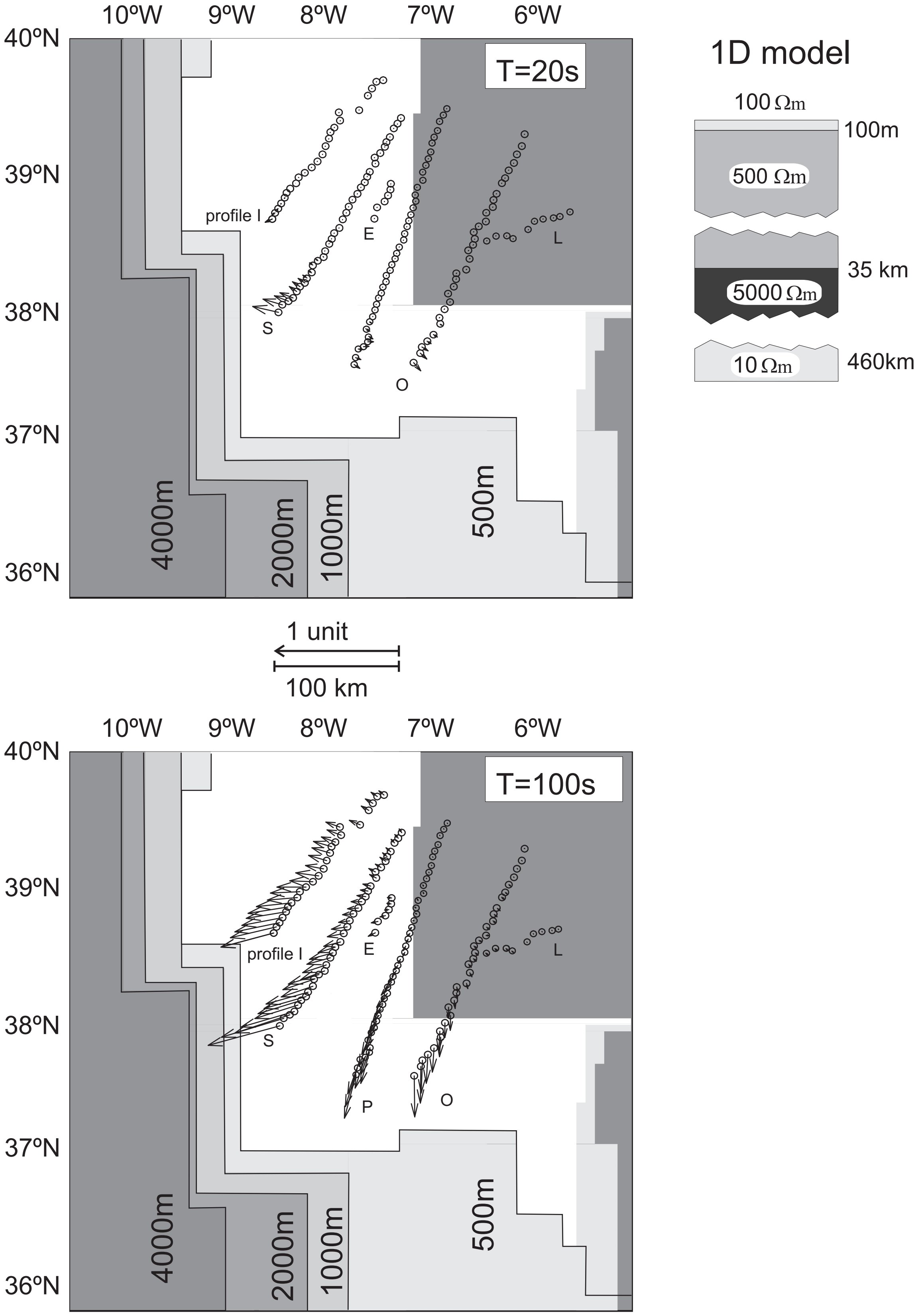

Figure 6. Plan view of the model used for the study of the ocean effect, including the bathymetry. The land part is represented by a 1D model (upper right panel). The induction arrows are shown in Parkinson convention at periods of 20 s and 100 s.

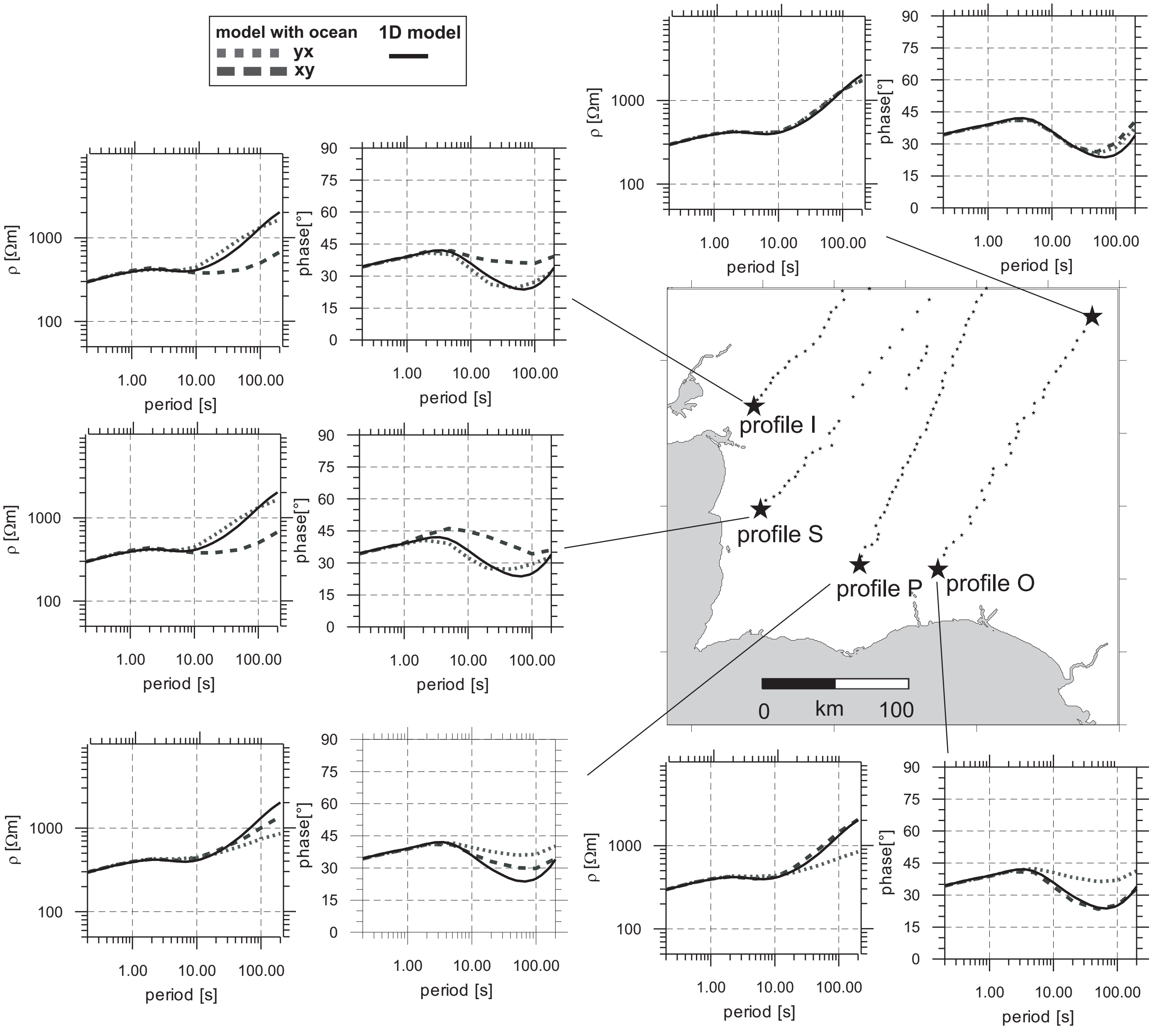

Figure 7. Ocean effect in the apparent resistivity and phase curves for the sites closest to the sea at each profile and one site located far away from the ocean (marked with a star). The solid line represents the response of the 1D land model.

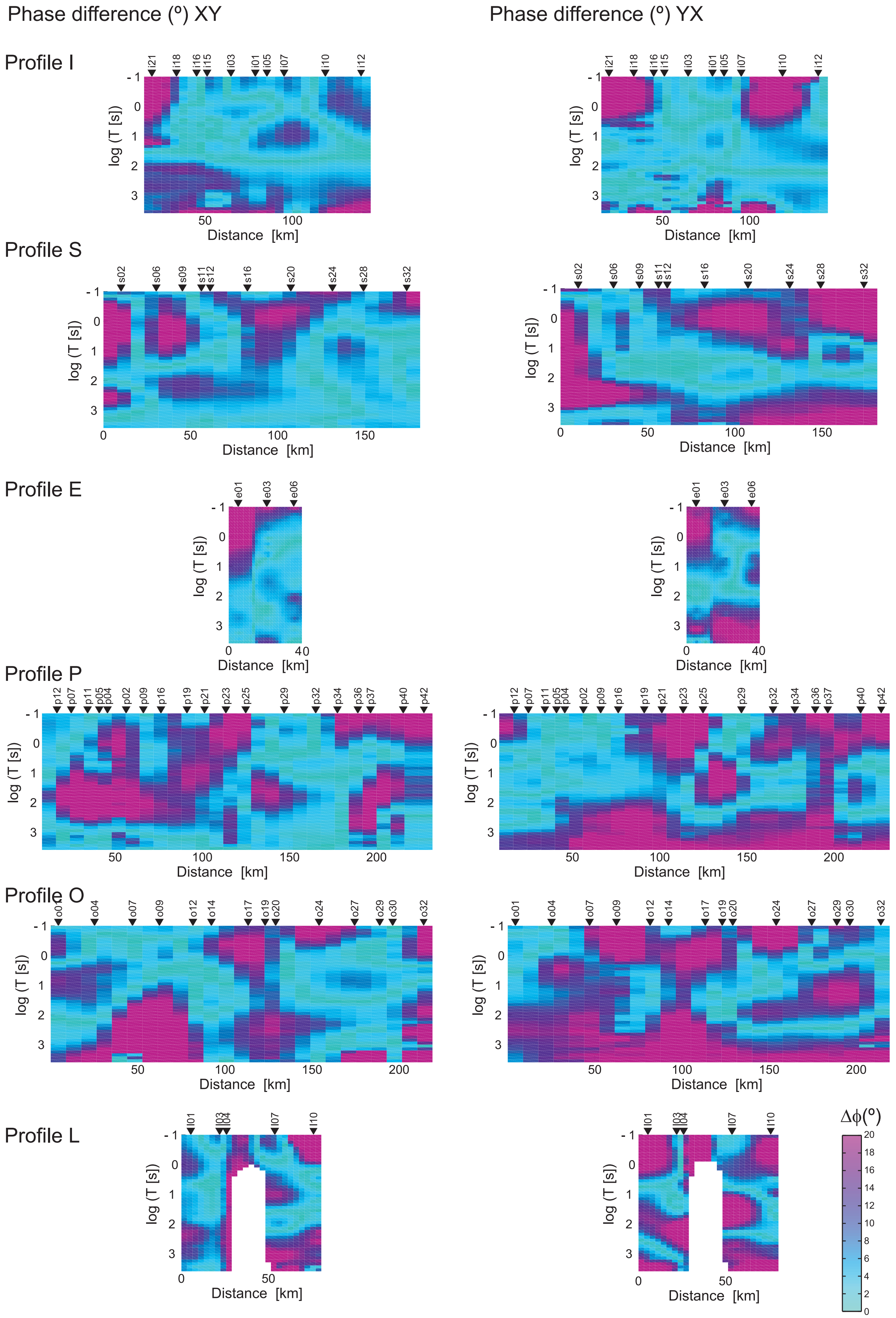

Figure 8. Pseudo-sections of the absolute phase difference between data and model responses for all the profiles.

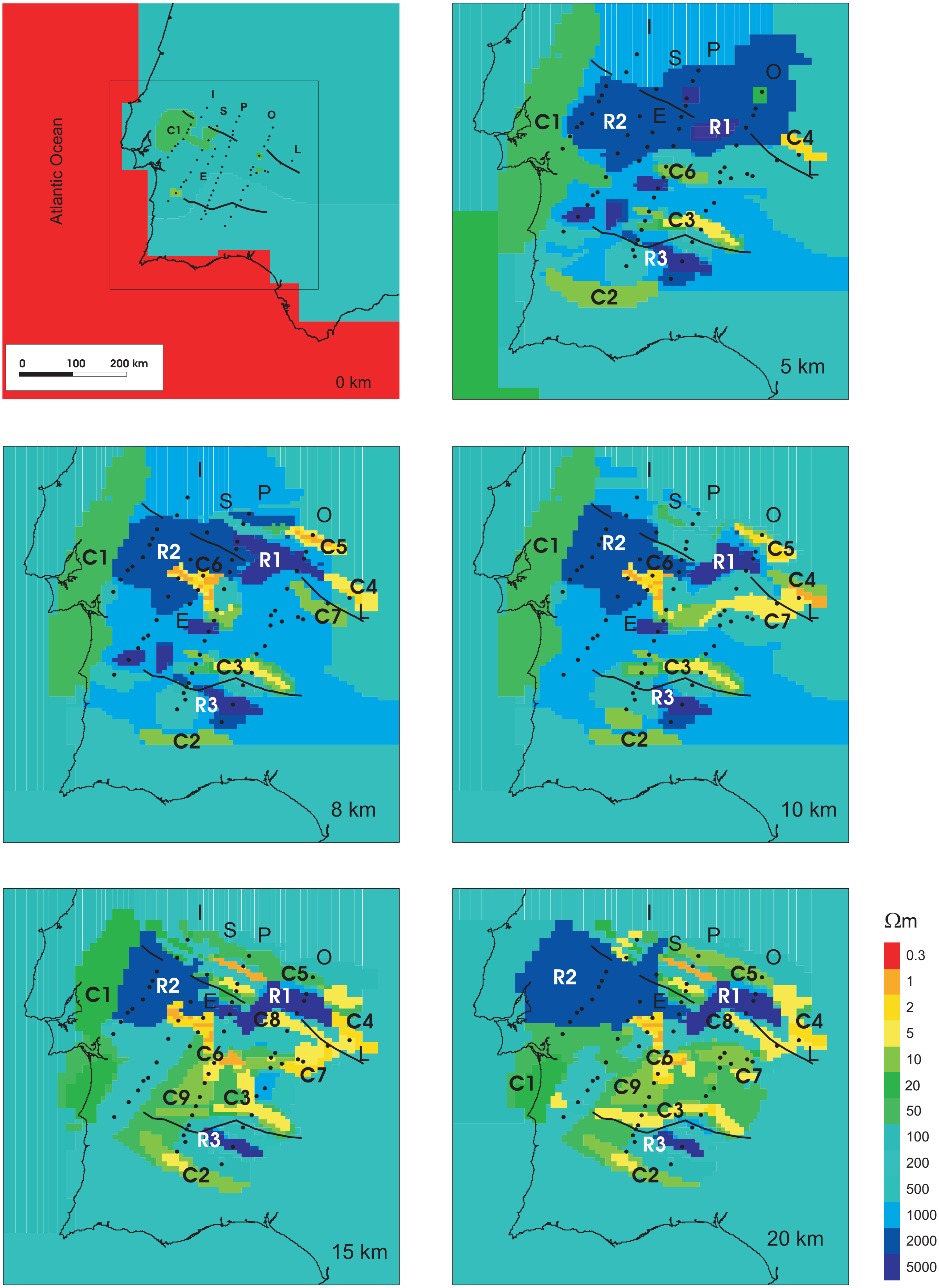

Figure 9. 3D electrical resistivity model. Plan view at different depths. The black dots indicate the location of the MT sites used for the study. The shore line and the surface occurrence of the SPZ/OMZ and OMZ/CIZ sutures (see figures 2 and 3) are shown to facilitate the location of the structures.

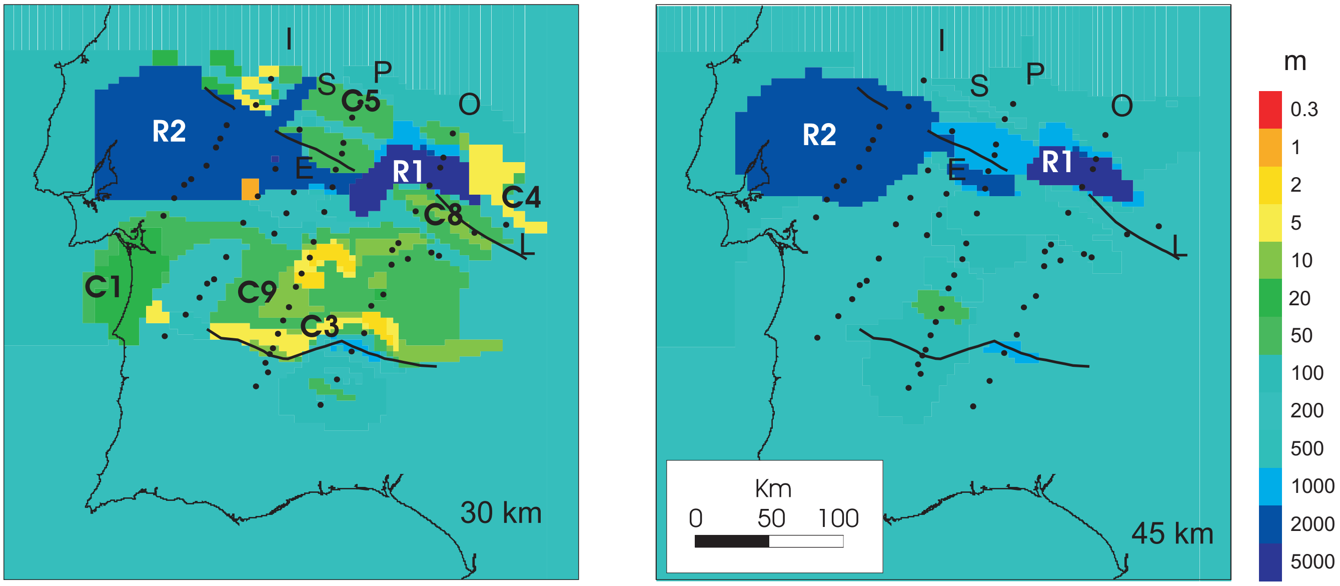

Figure 9 (cont.).

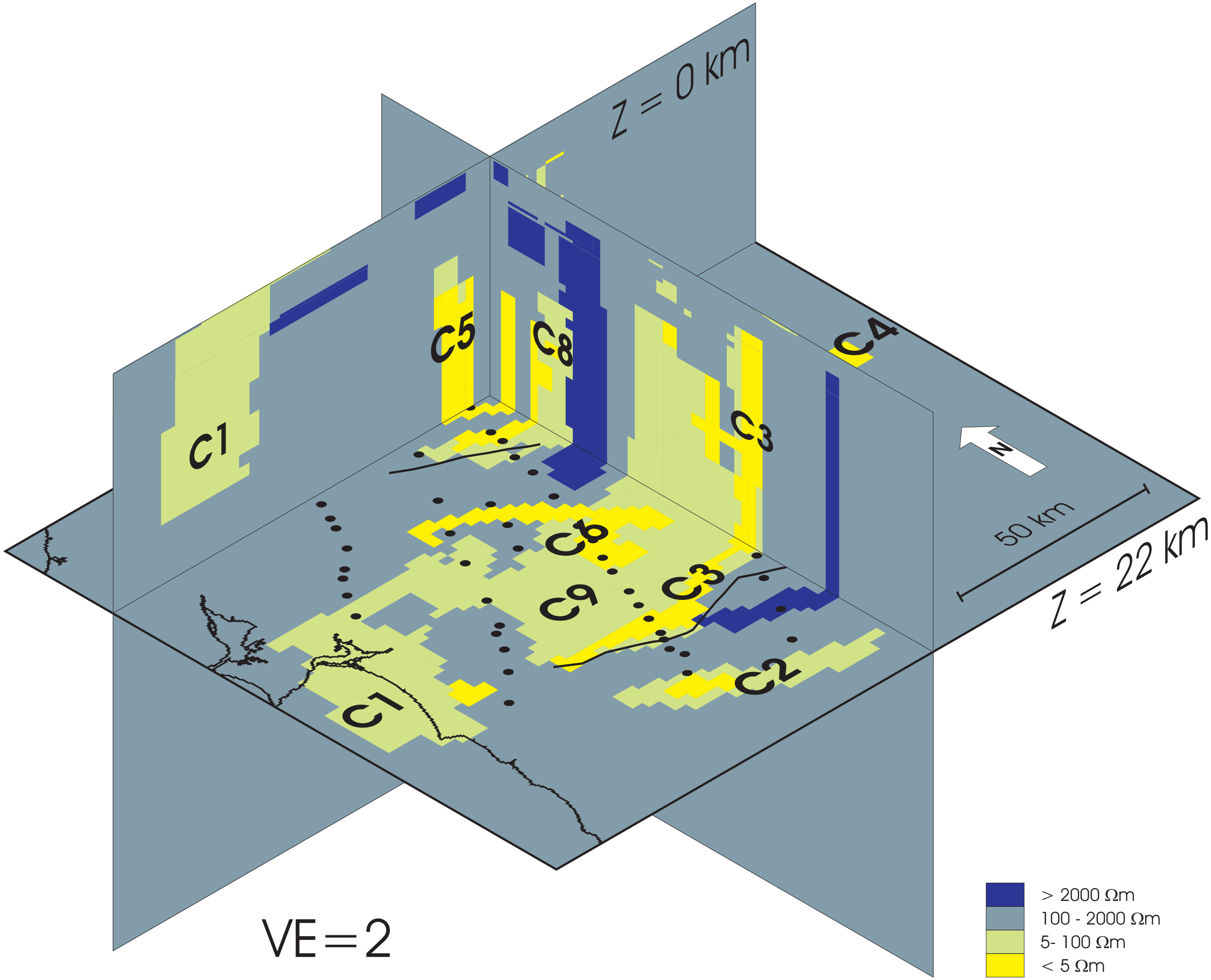

Figure 10. Plan view of the model at a depth of 22 km and two cross sections along a NS profile and an EW profile (Vertical exageration = 2). The resistivity values have been grouped to highlight the most striking conductivity features. Conductors C1, C3 and C6 merge into the conductive layer C9. The black dots indicate the location of the MT sites. The shoreline and the surface occurrence of the sutures SPZ/OMZ and OMZ/CIZ (see figures 2 and 3) are shown to facilitate the location.

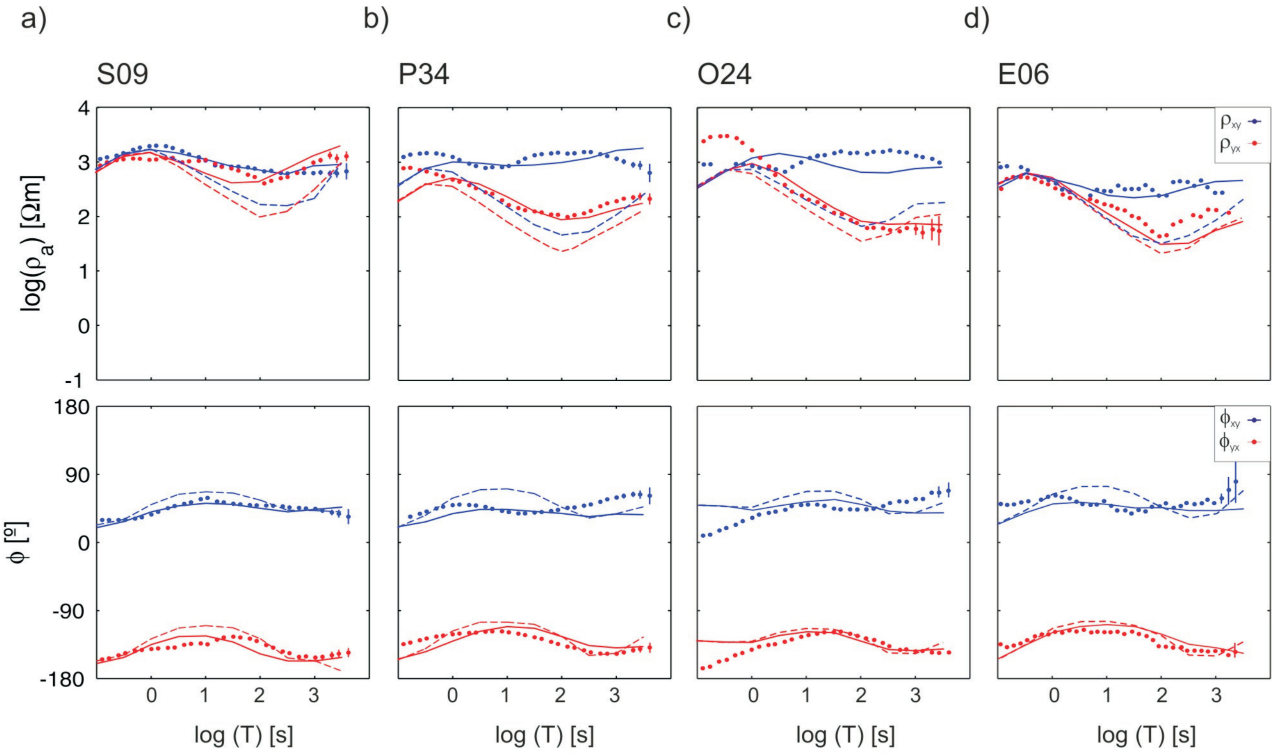

Figure 11. Data and model responses for different sensitivity tests. The dots represent the data, the solid lines the responses of the final model (Figs. 9, 10) and the dashed lines the responses of the altered models: a) Without the resisitive interruption of conductor C3 in the south of profile S. b) and c) With a 20 Ωm layer extending from 10 to 30 km instead of the complex conductive structure. d) With conductor C6 replaced by a more extended 20 Ωm conductive body.